Microtubule Sliding within the Bridging Fiber Pushes Kinetochore Fibers Apart to Segregate Chromosomes

Vukušić, Kruno; Buđa, Renata; Bosilj, Agneza; Milas, Ana; Pavin, Nenad; Tolić, Iva Marija

Article

Developmental Cell

Microtubule Sliding within the Bridging Fiber Pushes Kinetochore Fibers Apart to Segregate Chromosomes

Graphical Abstract

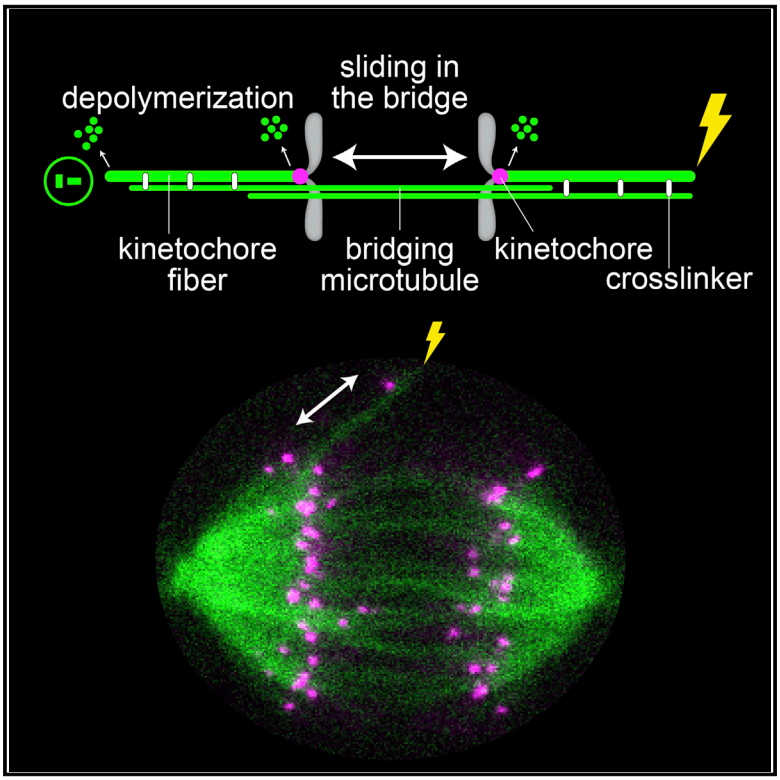

Highlights

- Kinetochores can segregate without any connection to one spindle pole
- Bridging fibers are required for proper kinetochore and spindle pole separation
- Kinetochore and bridging fibers are crosslinked and slide together during anaphase
- Sliding in the bridging fiber is one of the anaphase mechanisms in human cells

Authors

Kruno Vukušić, Renata Buđa, Agneza Bosilj, Ana Milas, Nenad Pavin, Iva M. Tolić

Correspondence

npavin@phy.hr (N.P.), tolic@irb.hr (I.M.T.)

In Brief

The forces that drive chromosome segregation in mitosis in human cells remain poorly understood. Vukušić, Buđa et al. combine laser ablation, photoactivation, and theory to uncover a key role for bridging fibers, non-kinetochore microtubule bundles, in spindle pole separation. Forces from kinetochore and bridging fiber crosslinking contribute to chromosome segregation.

Vukušić et al., 2017, Developmental Cell *43*, 11–23
October 9, 2017
https://doi.org/10.1016/j.devcel.2017.09.010

Developmental Cell
Article

Microtubule Sliding within the Bridging Fiber Pushes Kinetochore Fibers Apart to Segregate Chromosomes

Kruno Vukušić,[1,3] Renata Buđa,[1,3] Agneza Bosilj,[2] Ana Milas,[1] Nenad Pavin,[2,*] and Iva M. Tolić[1,4,*]
[1]Division of Molecular Biology, Ruđer Bošković Institute, Bijenička cesta 54, 10000 Zagreb, Croatia
[2]Department of Physics, Faculty of Science, University of Zagreb, Bijenička cesta 32, 10000 Zagreb, Croatia
[3]These authors contributed equally
[4]Lead Contact
*Correspondence: npavin@phy.hr (N.P.), tolic@irb.hr (I.M.T.)
https://doi.org/10.1016/j.devcel.2017.09.010

SUMMARY

During cell division, mitotic spindle microtubules segregate chromosomes by exerting forces on kinetochores. What forces drive chromosome segregation in anaphase remains a central question. The current model for anaphase in human cells includes shortening of kinetochore fibers and separation of spindle poles. Both processes require kinetochores to be linked with the poles. Here we show, by combining laser ablation, photoactivation, and theoretical modeling, that kinetochores can separate without any attachment to one spindle pole. This separation requires the bridging fiber, a microtubule bundle that connects sister kinetochore fibers. Bridging fiber microtubules in intact spindles slide apart with kinetochore fibers, indicating strong crosslinks between them. We conclude that sliding of microtubules within the bridging fibers drives pole separation and pushes kinetochore fibers poleward by the friction of passive crosslinks between these fibers. Thus, sliding within the bridging fiber works together with the shortening of kinetochore fibers to segregate chromosomes.

INTRODUCTION

To segregate chromosomes in mitosis, spindle microtubules (MTs) exert forces on kinetochores to move them apart in a process known as anaphase (Maiato and Lince-Faria, 2010). Anaphase relies on multiple mechanisms, even within an individual cell. In most model systems, segregation includes chromosome-to-pole motility (anaphase A) and spindle elongation (anaphase B) (Asbury, 2017; McIntosh et al., 2012; Pavin and Tolic, 2016; Scholey et al., 2016). Two mechanisms that contribute to anaphase A are the Pac-Man activity, whereby kinetochores stimulate the depolymerization of kinetochore fibers (K-fibers) at their plus ends and move toward the spindle pole by "chewing them up" (Gorbsky et al., 1987; Mitchison et al., 1986), and poleward flux of K-fibers, i.e., their translation toward the spindle pole accompanied by disassembly at the pole (Mitchison, 1989; Mitchison and Salmon, 1992). Sliding of overlap MTs (Saxton and McIntosh, 1987) and pulling from the cortex on astral MTs (Aist et al., 1993; Grill et al., 2001) drive spindle pole separation in anaphase B, and thus also contribute to kinetochore separation. To generate forces for chromosome motion, these processes require direct or indirect connections of kinetochores with the spindle pole, defined as a broad region where the microtubule bundles are focused, whereas a direct linkage with centrosomes has been shown to be redundant in anaphase (Hiramoto and Nakano, 1988; Nicklas, 1989; Sikirzhytski et al., 2014). Despite intense research on anaphase in a variety of model organisms, the mechanisms driving chromosome segregation in human cells are not well known.

Previous research on anaphase in human cells have marked the importance of dynamic ends of K-fibers in chromosome motion (Ganem et al., 2005; Sikirzhytski et al., 2014; Stumpff et al., 2008; Yang et al., 2007). However, sister K-fibers are linked laterally along their length with an antiparallel interpolar MT bundle termed bridging fiber (Kajtez et al., 2016; Milas and Tolić, 2016; Tolić, 2017; Tolic and Pavin, 2016). Similar interpolar microtubules have been observed in the vicinity of K-fibers and between sister kinetochores in electron microscopy images of PtK1 and human spindles in metaphase (Mastronarde et al., 1993; McDonald et al., 1992; McIntosh and Landis, 1971; Nixon et al., 2017). Recent work has shown that almost all interpolar MT bundles are associated with kinetochores and act as a bridge between sister K-fibers in metaphase (Polak et al., 2017). Because of their antiparallel organization and their attachment to sister K-fibers, bridging fibers may have a role in anaphase kinetochore separation.

In the current study, by combining live-cell imaging, laser cutting of MT bundles, photoactivatable GFP experiments, and theoretical modeling, we find that sliding of the MTs within the bridging fiber pushes sister K-fibers apart, thereby separating sister kinetochores. The bridging fibers are also crucial for the separation of spindle poles, whereas pulling from the cortex does not play a significant role. By measuring the poleward flux, Pac-Man, and sliding activities, we determine that half of the chromosome segregation velocity can be attributed to sliding between bridging MTs. By combining our experimental results with a theoretical model, we conclude that sliding of bridging MTs, that pushes K-fibers poleward through the friction

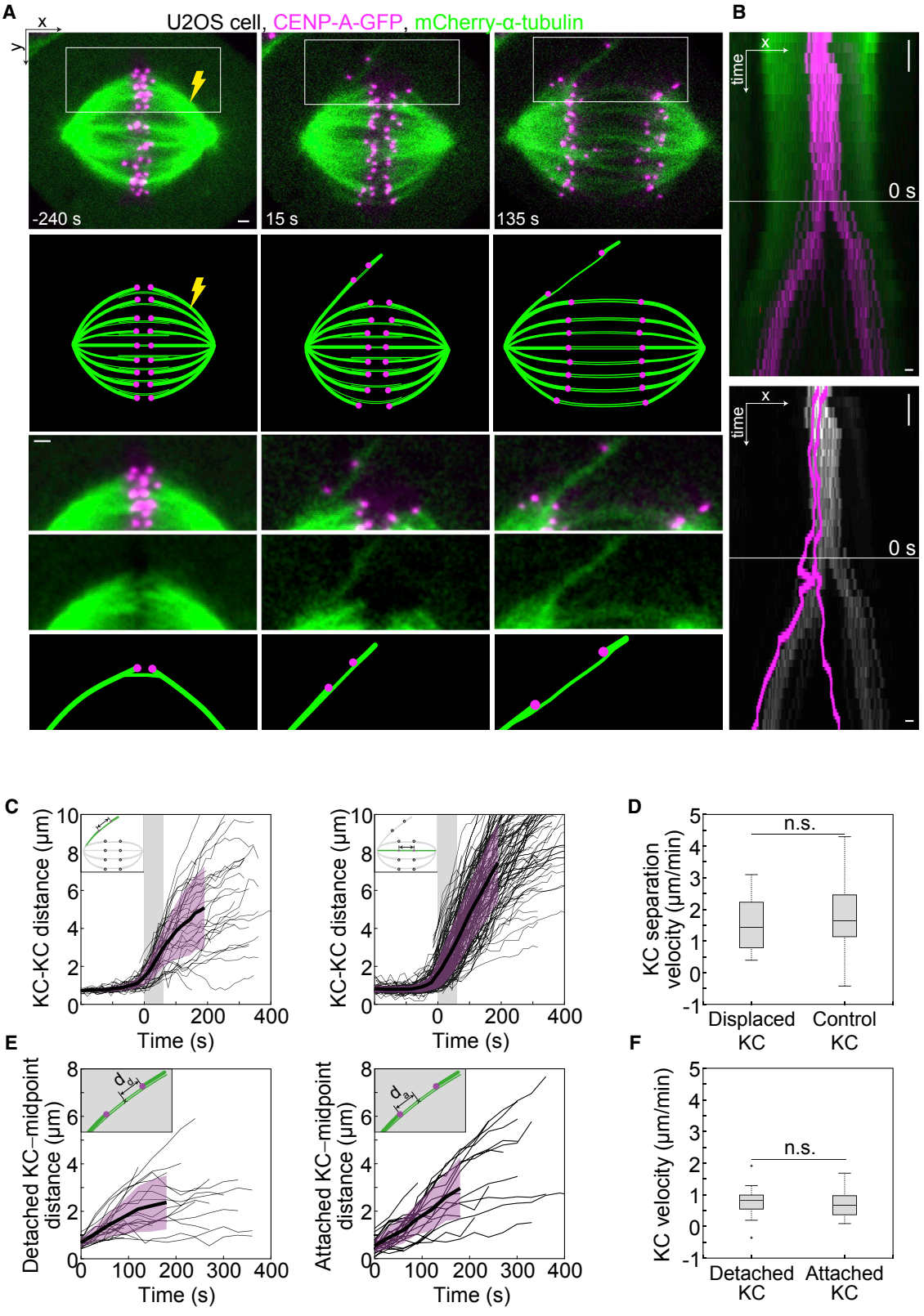

(legend on next page)

of crosslinks between them, is one of the mechanisms for chromosome movement in human cells.

RESULTS

Assay for Dynamics of Anaphase Kinetochores Lacking Connection to One Spindle Pole

We set out to determine the function of bridging MTs in chromosome segregation by disconnecting a pair of sister kinetochores, along with the corresponding K-fibers, from one spindle pole. We imaged live human U2OS cells stably expressing the centromere protein CENP-A-GFP, mCherry-α-tubulin, and photoactivatable (PA)-GFP-tubulin. We severed one of the outermost K-fibers about 2.5 μm away from the kinetochore in late metaphase (Figures 1A, 1B, S1A, and S1B). Outermost K-fibers were selected for ablation because they move away from the spindle after the cut (Kajtez et al., 2016) (Figures 1A and S1A), which helped us to distinguish a single kinetochore pair and the associated MTs from their neighbors. The distance of 2.5 μm away from the kinetochore was chosen to preserve the connection between the bridging fiber and the K-fiber stub, given that the K-fiber and the bridging fiber merge 1–2 μm away from the kinetochore (Kajtez et al., 2016; Milas and Tolić, 2016). Cutting was done in late metaphase in order to follow the movements of displaced kinetochores from the onset of anaphase, and to maximize the post-severing movement of the kinetochores away from the spindle (Figure S1C). After severing, in 90% of the cells the K-fiber stub was pulled back toward the spindle pole before anaphase onset, presumably by dynein-mediated transport (Elting et al., 2014; Sikirzhytski et al., 2014). We analyzed only those cells in which the kinetochores remained without a connection to one spindle pole at least until mid-anaphase, and in which the direction of kinetochore and stub movement was away from the pole from which it was disconnected (Figure S1D). We will refer to such kinetochores as displaced kinetochores. Analysis of the MT signal intensity indicated that the bridging fiber between displaced kinetochores remained preserved after anaphase onset (Figures S1E and S1F). In addition, silicon rhodamine (SiR)-tubulin labeling (Lukinavicius et al., 2014) and α-tubulin immunostaining showed the bridging fiber preservation between displaced kinetochores (Figure S1G). To see whether other interpolar MT bundles are found close to the displaced kinetochores, we used protein regulator of cytokinesis 1 (PRC1), which binds to antiparallel overlap regions (Jiang et al., 1998; Kajtez et al., 2016; Mollinari et al., 2002; Polak et al., 2017). We found PRC1 between the kinetochores before and after ablation, from metaphase throughout anaphase, whereas other PRC1-labeled overlap bundles were not visible in the vicinity of the displaced kinetochores (Figure S1H).

Kinetochores Can Segregate Independently of the Attachment to One Spindle Pole

Interestingly, at the onset of anaphase the displaced sister kinetochores started to separate, similar to the other kinetochore pairs in the spindle (Figures 1A, 1B, S1A, and S1B; Movie S1). To quantify kinetochore movements, we tracked the displaced kinetochores until the end of anaphase or until their stub became reintegrated into the spindle, whichever occurred first. Control kinetochores, whose K-fibers were not severed, were tracked until the end of anaphase in the same spindle. We found that the displaced sister kinetochores separated at a velocity of 1.53 ± 0.12 μm/min (results are mean ± SEM unless otherwise indicated, n = 39 cells) during the first 60 s after anaphase onset (Figure 1C [left panel] and Table 1). This velocity was similar to the segregation velocity of control kinetochores, 1.77 ± 0.08 μm/min (n = 39, p = 0.51; Figures 1C [right panel] and 1D; Table 1). Thus, sister kinetochores segregate with the unchanged velocity when one of them is disconnected from the spindle pole.

The observed segregation of displaced kinetochores may be a result of the movement of both sister kinetochores away from each other, or may be primarily the result of the movement of the kinetochore with the intact K-fiber, while the other kinetochore remained stationary after its K-fiber was severed. To evaluate the contribution of each sister kinetochore to their segregation, we used the midpoint between the displaced sister kinetochores at the beginning of anaphase as the fixed reference point from which their distance was measured (Figure S1I). This choice of the reference point was justified because the sister kinetochore axis remained close to the midpoint during early anaphase (Figure S1J). We found that, once both sister kinetochores started to move, they moved with similar velocities (v = 0.76 ± 0.09 μm/min and 0.65 ± 0.08 μm/min for the kinetochore with the severed and the intact K-fiber, respectively; n = 24, p = 0.33) (Figures 1E and 1F; Table 1). We conclude that not only the

Figure 1. Kinetochore Segregation without Attachment to One Spindle Pole

(A) Time-lapse images of the spindle (first row) in a U2OS cell-expressing centromere protein CENP-A-GFP (magenta) and mCherry-α-tubulin (green), and smoothed enlargements of the boxed region (third row, fourth row only in green channel). Schemes are shown under the images. K-fiber was cut 2.5 μm from the kinetochore in metaphase (yellow lightning bolt). Time 0 is anaphase start.

(B) Kymograph (consecutive maximum-intensity projections onto the y axis) of the spindle from (A) showing merged channels (top), and traces of displaced kinetochores in magenta and control kinetochores in gray (bottom).

(C) Distance between displaced (left, n = 41 kinetochore pair from 39 cells) and control (right, n = 137 kinetochore pairs from 39 cells) sister kinetochores (see schemes) over time, where time 0 is anaphase onset. Individual kinetochore pairs (thin lines), mean (thick line), SD (pink region), and time interval for velocity measurements (gray region).

(D) Box plot of velocities of displaced and control kinetochores. In the box plot, the central mark indicates the median, with the bottom and top edges of the box indicating the 25th and 75th percentiles, respectively. The whiskers extend to the most extreme data points, with exception of the outliers that are marked individually with the plus symbol.

(E) Distance between detached (left, d_d on scheme, n = 24 kinetochore pairs) and attached (right, d_a on scheme, n = 24 kinetochore pairs) displaced kinetochores from their midpoint defined at the beginning of anaphase. Further details as in (C).

(F) Box plot of velocities of detached and attached displaced kinetochores from their midpoint. Measures as in (D).

KC, kinetochore. Data were statistically analyzed using a t test (n.s., not significant). Scale bars, 1 μm; time bars, 1 min. See also Figure S1.

Table 1. List of Velocities Obtained from Experimental Measurements

Experiment	Parameter	Mean ± SEM (μm min^{-1}) (No. of Cells, No. of Kinetochore Pairs)		p Value
Cut 2.5 μm[c]		Displaced	Control	
	kinetochore-kinetochore	1.53 ± 0.12 (39, 41)	1.77 ± 0.08 (39, 137)	0.51
	kinetochore-midpoint	0.76 ± 0.09 (24, NA)[a]	NA	0.33
		0.65 ± 0.08 (24, NA)[b]		
	intact pole-kinetochore	0.57 ± 0.09 (24, NA)[a]	0.47 ± 0.05 (24, NA)	0.34
	intact pole-stub tip	0.80 ± 0.12 (24, NA)	NA	NA
	kinetochore-stub tip	0.24 ± 0.12 (14, NA)[b]	NA	NA
	sliding within the bridging fiber	2.13 ± 0.33 (5, NA)	2.08 ± 0.18 (25, NA)	0.77
Cut 2.5 μm + bridge cut[c]	kinetochore-kinetochore	0.49 ± 0.01 (14, 14)	1.54 ± 0.02 (14, 55)	3.2×10^{-4}
Cut 1 μm[c]	kinetochore-kinetochore	0.28 ± 0.01 (10, 10)	1.51 ± 0.02 (10, 30)	3.6×10^{-5}
Midzone cut[d]		Midzone Cut	Control	
	kinetochore-kinetochore	1.30 ± 0.16 (11,11)	2.30 ± 0.13 (24, 24)	6.6×10^{-3}
	pole-pole	0.52 ± 0.10 (11, NA)	1.19 ± 0.07 (24, NA)	4.3×10^{-5}
	pole-kinetochore	0.57 ± 0.08 (11, NA)	0.50 ± 0.05 (24, NA)	0.57
Astral cut[d]		Astral Cut	Control	
	kinetochore-kinetochore	2.40 ± 0.13 (10, 29)	2.30 ± 0.13 (24, 24)	0.21
	pole-pole	1.36 ± 0.10 (10, NA)	1.19 ± 0.07 (24, NA)	0.57
Intact spindle[c]		Bridging Fiber	K-Fiber	
	sliding	2.08 ± 0.18 (25, NA)	1.88 ± 0.19 (25, NA)	0.44
	poleward flux	0.42 ± 0.06 (25, NA)	0.32 ± 0.05 (25, NA)	0.19
	sliding	STLC	Control	
		1.55 ± 0.47 (11, NA)	2.0 ± 0.63 (10, NA)	0.21
		KIF15 siRNA		
		1.54 ± 0.43 (11, NA)	2.0 ± 0.63 (13, NA)	0.21
		STLC + KIF15 siRNA		
		1.53 ± 0.44 (11, NA)	2.0 ± 0.63 (10, NA)	0.19
		MKLP1 siRNA	Control	
	kinetochore-kinetochore	1.63 ± 0.19 (14, 50)	2.25 ± 0.26 (23, 72)	6×10^{-6}
	pole-pole	0.91 ± 0.11 (14, NA)	1.31 ± 0.15 (23, NA)	0.0048

Velocities of various anaphase movements measured from different experimental approaches are shown. The velocities were statistically compared between control and experimentally modified groups (by laser ablation or protein depletion), where applicable. NA, not applicable.
[a]Attached displaced kinetochore.
[b]Detached displaced kinetochore.
[c]Measured in 1-min intervals.
[d]Measured in 3-min intervals.

kinetochore with the intact K-fiber but also the one with the severed K-fiber contributes to their segregation during anaphase.

Bridging Fiber Is Required for the Separation of Displaced Kinetochores

To distinguish whether the bridging fiber or other structures are crucial for the separation of displaced kinetochores, we used laser ablation to sever the bridging fiber. Hence, we devised a double-ablation assay in which we first severed a K-fiber as described above. Once the displaced sister kinetochores started to separate, we ablated a point between them to sever the bridging fiber (Figures 2A and S2A). In contrast to the single-ablation experiments, kinetochores did not continue to segregate after double ablation. In 10 out of 14 cells both displaced sister kinetochores moved together toward the spindle pole of the intact K-fiber (Figures 2A, 2B, S2A, and S2B; Movie S2A). This joint movement may be due to entanglement of the chromosome arms. In the remaining cells, the K-fiber stub and the accompanying kinetochore were pulled by other spindle MTs toward either spindle pole, as observed previously in metaphase (Elting et al., 2014; Sikirzhytski et al., 2014). To quantify kinetochore movements in experiments where the bridging fiber was disrupted, we measured displaced kinetochore segregation velocity during 60 s after severing, $v_s = 0.49 \pm 0.01$ μm/min (n = 14, Table 1). This velocity was significantly lower in comparison with the displaced kinetochores with an intact bridging fiber (v_s = 1.53 ± 0.12 μm/min, n = 39, $p = 1.3 \times 10^{-3}$; Figure 1D) and control sister kinetochores on the unperturbed side of the same spindle ($v_s = 1.54 \pm 0.02$ μm/min, n = 14, $p = 3.2 \times 10^{-4}$; Figure 2C and Table 1). Collectively, these results show that severance of

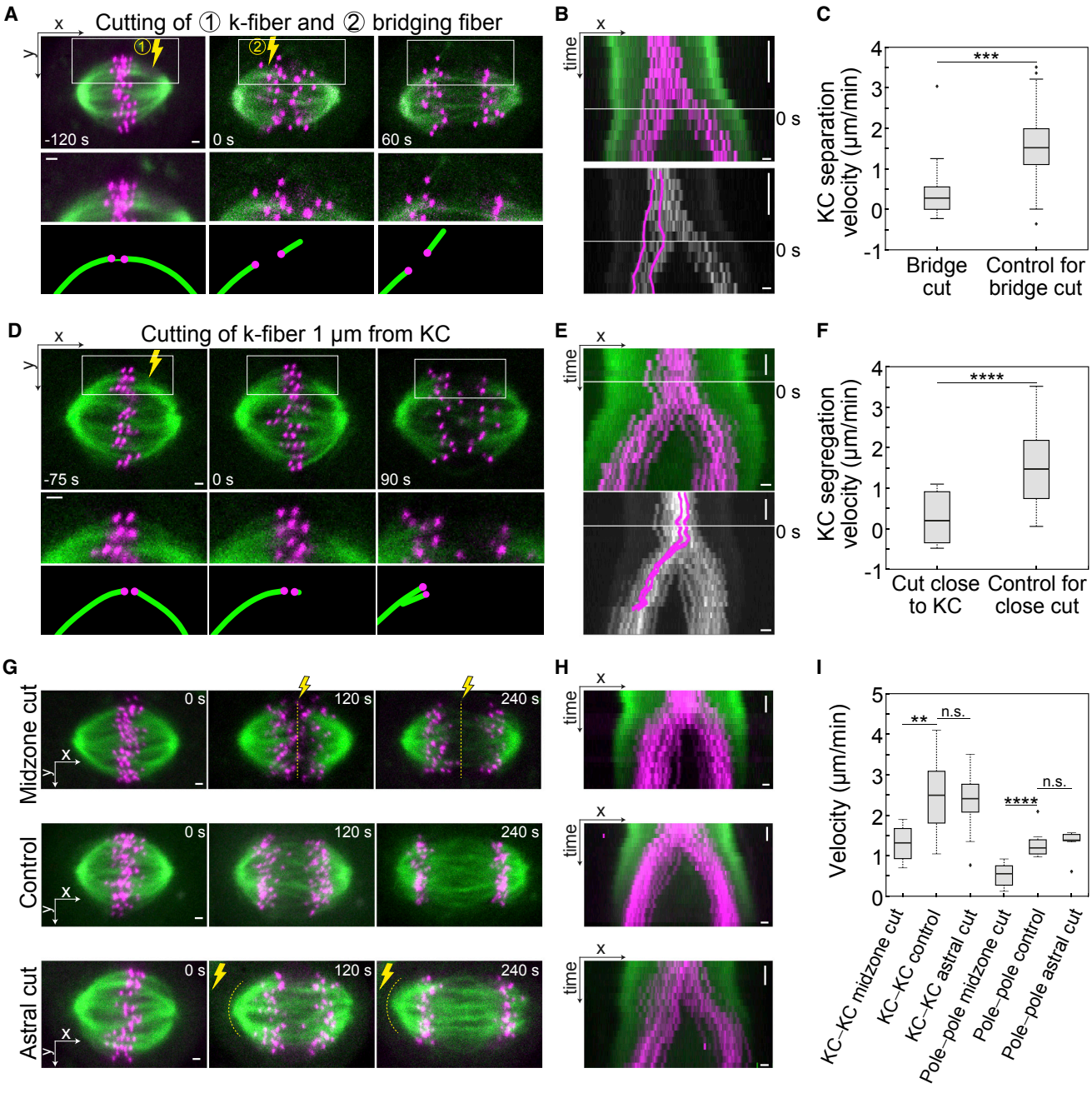

Figure 2. Bridging Fiber Is Required for the Separation of Displaced Kinetochores and Normal Separation of Spindle Poles

(A) Time-lapse images of the spindle in a U2OS cell: before the K-fiber was cut 2.5 μm from the kinetochore (top left, yellow sign marks the cut), when the bridging fiber was cut (top center, time 0, yellow sign marks the cut) at the beginning of anaphase, and 60 s later (top right). Enlargements of the boxed region (middle row) and schemes (bottom; MTs, green; kinetochores, magenta).

(B) Kymograph of the spindle from (A) showing merged channels (top) and traces of displaced kinetochores in magenta and control kinetochores in gray (bottom).

(C) Box plot of velocities of displaced and control kinetochores. In the box plot, the central mark indicates the median, with the bottom and top edges of the box indicating the 25th and 75th percentiles, respectively. The whiskers extend to the most extreme data points, with exception of the outliers that are marked individually with the plus symbol. ***$p < 0.001$.

(D) Time-lapse images of the spindle in a U2OS cell before the K-fiber was cut 1 μm from the kinetochore (top left, yellow sign marks the cut), at the beginning of anaphase (top center, time 0), and 90 s later (top right). Enlargements of the boxed region (middle row) and schemes (bottom).

(E) Kymograph of the spindle from (D). Description as in (B).

(F) Box plot of velocities of displaced and control kinetochores. Measures as in (C). ****$p < 0.0001$.

(legend continued on next page)

the bridging fiber disrupted kinetochore separation. We conclude that the bridging fiber is required for proper segregation of displaced kinetochores.

To explore the role of the K-fiber stub that remains attached to the kinetochore after the severing, we severed the outermost spindle element close to the kinetochore (~1.0 μm away) during late metaphase (Figure 2D). We expected that such short stubs would become disconnected from the bridging fiber, given that the K-fiber and the bridging fiber merge 1–2 μm away from the kinetochore (Kajtez et al., 2016; Milas and Tolić, 2016). In 6 out of 10 cells, we observed movement of the accompanied kinetochore toward the opposite spindle pole (Figures 2D and 2E; Movie S2B), whereas in the remaining cells both displaced sister kinetochores continued to move together toward the intact spindle pole (Figures S2C and S2D), similarly to the experiments in which the bridging fiber was severed. The velocity of kinetochores with a short K-fiber stub (<1 μm) was 0.28 ± 0.01 μm/min (n = 10, Table 1), which is significantly lower in comparison with the displaced kinetochores with a long stub (>2.5 μm, 1.53 ± 0.12 μm/min, n = 39, $p = 1.9 \times 10^{-4}$; Figure 1D) and control sister kinetochores on the unperturbed side of the same spindle (1.51 ± 0.02 μm/min, n = 10, $p = 3.6 \times 10^{-5}$; Figure 2F and Table 1). These results imply that a short K-fiber stub is not able to maintain the connection with the bridging fiber, resulting in impaired kinetochore segregation.

Bridging Fibers Are Required for Proper Spindle Pole Separation

To test the contribution of all bridging fibers to kinetochore separation, we applied the laser ablation assay to cut the midzone region between all sister kinetochores (Figure 2G). Based on the finding that in metaphase almost all interpolar MT bundles are bridging fibers linking a pair of kinetochores (Polak et al., 2017), we assume that this is the case also in early anaphase, meaning that almost all MT bundles in the midzone are bridging fibers. Midzone ablation resulted in a slower separation of kinetochores and of the spindle poles (Figures 2G and 2H; Movie S2C). During the first 3 min of continuous midzone cutting, kinetochores segregated at a velocity of $v_s = 1.30 \pm 0.16$ μm/min (n = 11) and the poles at a velocity $v_p = 0.52 \pm 0.10$ μm/min (n = 11; Figure 2I and Table 1). These values were significantly lower than the respective values for control spindles, $v_s = 2.30 \pm 0.13$ μm/min (n = 24) and $v_p = 1.19 \pm 0.07$ μm/min (n = 24) ($p = 6.6 \times 10^{-3}$ and 4.3×10^{-5}, respectively) (Figures 2G–2I and S2E; Table 1). Continuous ablation most likely did not have a non-specific impact on anaphase because velocities of the kinetochore poleward movement were indistinguishable from control values (Figure S2F and Table 1), and the kinetochore separation velocities during continuous ablation of astral MTs were not different from control values (Figures 2I and S2E; Table 1). These results suggest that the slower kinetochore and pole separation is indeed the result of the disruption of bridging fibers. However, kinetochores and spindle poles were not completely motionless, suggesting that not all bridging fibers were disrupted. Together, these findings support the view that bridging fibers are an important part of the machinery segregating kinetochores and separating spindle poles.

MTs within the Bridging Fiber Slide Apart during Anaphase

The finding that the bridging fiber is required for the segregation of displaced kinetochores prompted us to investigate the role of MT sliding and Pac-Man activity in this process. We measured the changes in the contour length of the structure consisting of the intact K-fiber, bridging fiber, and the K-fiber stub of the displaced kinetochores, after severing the K-fiber ~2.5 μm away from the kinetochore (Figure 3A). This contour increased in length at a velocity of 0.80 ± 0.12 μm/min during the first 2 min of anaphase (n = 24) (Figures 3B and 3F; Table 1). At the same time, the intact K-fiber shortened at a velocity of 0.57 ± 0.09 μm/min (n = 24) (Figures 3C and 3F), which was similar to that of control K-fibers (Figure S3A and Table 1) and previous measurements (Yang et al., 2007). The K-fiber stub shortened at the velocity of 0.24 ± 0.12 μm/min (n = 14) (Figures 3D, 3F, and S3B; Table 1). A similar value (0.22 ± 0.11 μm/min, n = 9, p = 0.77) was obtained by analyzing a photoactivated spot at the stub minus end, which remained stable as the stub shortened, indicating that the stub shortening is a result of depolymerization at the plus end, i.e., Pac-Man activity (Figures S3C and S3D). Because 2 out of 3 segments of the contour shortened, the elongation of the total contour is most likely a consequence of the sliding apart of MTs within the bridging fiber.

To test directly whether bridging MTs, linked to displaced kinetochores, slide apart during anaphase, we photoactivated PA-GFP-tubulin within the bridging fiber after sister kinetochores started to separate. If the MTs within the bridging fiber slide apart, the photoactivated spot should split into two spots that move away from each other. Indeed, as the kinetochores segregated, we observed that the photoactivated spot separated into two spots (v = 2.13 ± 0.33 μm/min, n = 5) (Figures 3E, 3F, and S3E; Table 1).

To discover whether the MTs within the bridging fibers slide apart in intact spindles, we photoactivated PA-GFP-tubulin in a line across the spindle midzone during anaphase without performing laser ablation (Figure 4A and Movie S3). We observed that in intact spindles, as the anaphase continued, the initial photoactivated spot separated into two spots (v = 2.08 ± 0.18 μm/min, n = 25; Figure 4A and Table 1), similar to the spot between displaced kinetochores (p = 0.77, Figure 3F), indicating that the bridging MTs slide apart in intact spindles during anaphase.

To test the proteins that may drive or regulate MT sliding within the bridging fiber in anaphase, we used a candidate approach based on the known protein ability to slide antiparallel MTs and

(G) Time-lapse images of the spindle during midzone cut along the dotted yellow line (top), control anaphase spindle (middle), and during astral MT cut along the dotted yellow line (bottom) in a U2OS cell.

(H) Kymographs of the spindles from (G) showing merged channels.

(I) Box plot of kinetochore separation velocities (KC-KC) and pole separation velocities (pole-pole) for the conditions from (G). Measures as in (C). n.s., not significant. **p < 0.01, ****p < 0.0001.

Data were statistically analyzed using a t test. Scale bars, 1 μm; time bars, 1 min. See also Figure S2.

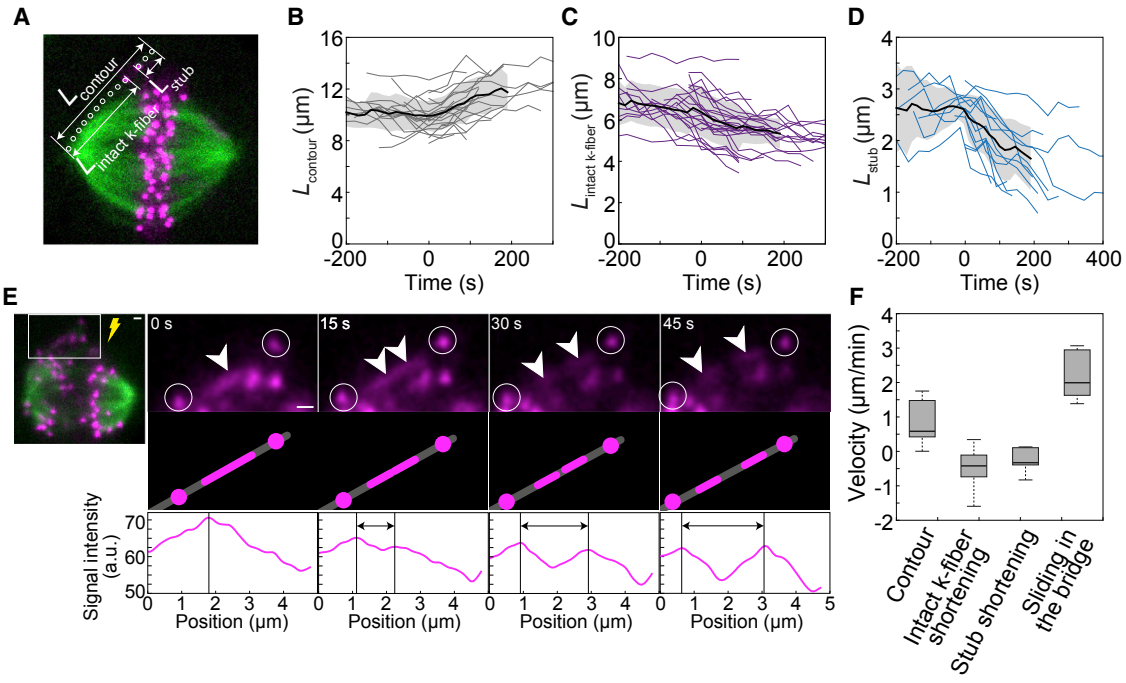

Figure 3. Bridging MTs Slide Apart between Displaced Kinetochores

(A) Image of the spindle in a U2OS cell showing tracking of the contour length of the intact K-fiber, $L_{\text{intact K-fiber}}$, K-fiber stub resulting from the ablation, L_{stub}, and the total contour, L_{contour}.

(B–D) L_{contour} (n = 14), $L_{\text{intact K-fiber}}$ (n = 24), and L_{stub} (n = 24), measured as shown in (A), over time. Time 0 is anaphase onset. Individual kinetochore pairs (thin lines), mean (thick line), SD (shaded region).

(E) Photoactivation of the bridging fiber between displaced kinetochores. Spindle after K-fiber ablation (left), smoothed enlargements of the boxed region in the channel showing CENP-A-GFP and PA-GFP-tubulin (magenta, top row) after photoactivation of the bridging fiber at time 0. White arrowheads mark the photoactivated spot, which splits into two spots. Circles mark the kinetochores. Schemes (middle row) show the kinetochores and the photoactivated regions in magenta and MTs in gray. Signal intensities of the PA-GFP-tubulin between the displaced sister kinetochores in the respective frames above (bottom row). Vertical lines mark the signal intensity peaks and arrowheads show the separation of the photoactivated spots.

(F) Box plot of velocities for parameters in (B), (C), (D), and (E), respectively. In the box plot, the central mark indicates the median, with the bottom and top edges of the box indicating the 25th and 75th percentiles, respectively. The whiskers extend to the most extreme data points, with exception of the outliers that are marked individually with the plus symbol.

Scale bars, 1 μm. See also Figure S3.

on the protein localization in the spindle midzone during anaphase. After inactivation of Eg5/KIF11 (kinesin-5) (Blangy et al., 1995; Kapitein et al., 2005; Sawin et al., 1992) by S-trityl-L-cysteine (STLC, see STAR Methods) (n = 11) (Skoufias et al., 2006), depletion of KIF15/Hklp2 (kinesin-12) (n = 14) (Tanenbaum et al., 2009; Vanneste et al., 2009) by small interfering RNA (siRNA) and combined Eg5 inhibition and KIF15 depletion (n = 10), the photoactivated spot in the spindle midzone separated into two spots at a velocity similar to that of control cells (Figure S4B and Table 1). These results suggest that Eg5 and KIF15 are not required for the sliding of bridging MTs in early anaphase. On the other hand, after depletion of mitotic kinesin-like protein 1 (MKLP1)/KIF23 (kinesin-6) (Mishima et al., 2002; Nislow et al., 1992), we were not able to measure the sliding velocity because the photoactivated spots were not detectable after 1 min as they were in controls (n = 10 for both conditions, Figures S4C and S4D), suggesting a higher MT turnover. Thus, it was not possible to distinguish the role of MKLP1 in microtubule sliding from its role in stabilization of bridging MTs. MKLP1 depletion resulted in a 28% decrease in kinetochore separation velocity (from 2.25 ± 0.26 μm/min to 1.63 ± 0.19 μm/min, n = 23, n = 14, $p = 6 \times 10^{-6}$) and a 30% decrease in pole separation velocity (from 1.31 ± 0.15 μm/min to 0.91 ± 0.11, n = 23, n = 14, p = 0.0048) when compared with untreated cells (Figures S4E and S4F; Table 1). These results indicate that MKLP1 contributes to the stabilization of the midzone and kinetochore separation in early anaphase.

K-Fibers Undergo Poleward Flux at the Same Velocity as the Bridging Fiber in the Intact Spindle

As the bridging MTs slide apart, the associated K-fibers may slide with respect to or together with them. To distinguish between these possibilities, we photoactivated K-fibers and bridging fibers in the same spindle (Figures 4B and S4A). We found that the photoactivated spots on the K-fiber moved apart at a velocity similar to that of the spots on the bridging fiber (1.88 ± 0.19 μm/min and 2.08 ± 0.18 μm/min, respectively; n = 25, p = 0.44) (Figure 4C and Table 1). Importantly, the two velocities were similar inside single cells, despite a significant variation in the rates of sliding among different cells

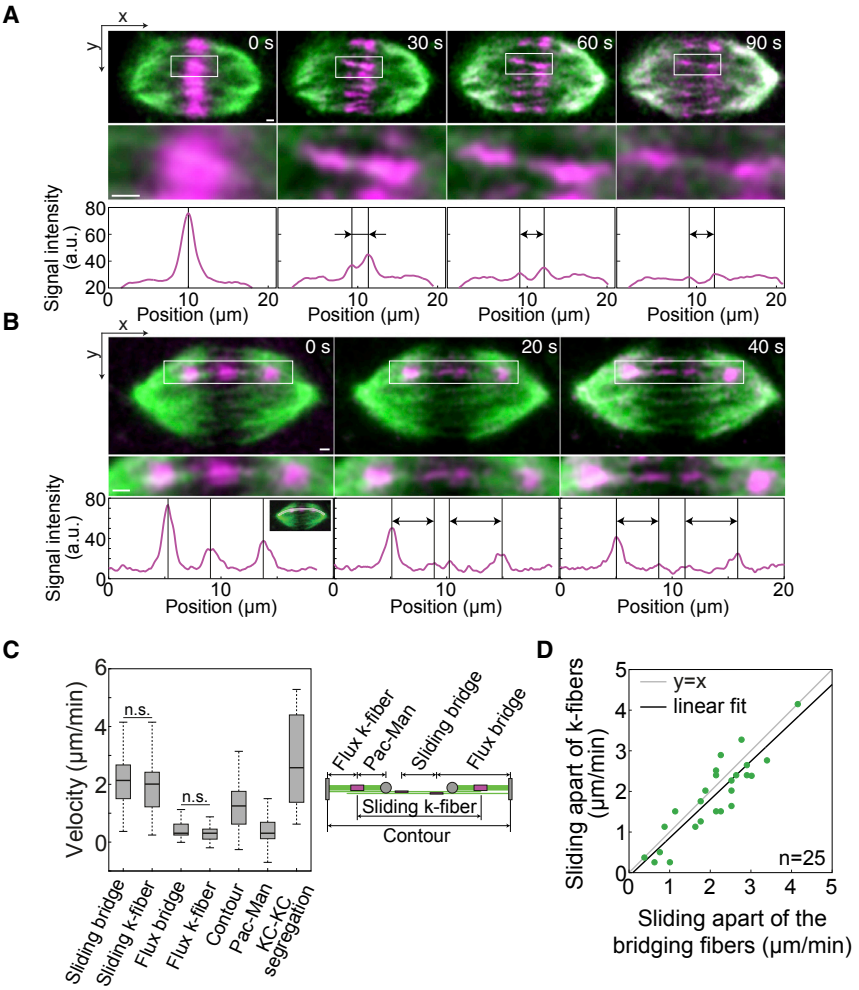

Figure 4. Bridging MTs Slide Apart Together with K-Fibers in Intact Spindles

(A and B) Photoactivation in intact spindles. Smoothed time-lapse images (top) of the anaphase spindle after photoactivation of PA-GFP-tubulin at time 0 within bridging fibers (A), or both bridging fibers and K-fibers (B). Enlargements of the boxed region (middle row) and signal intensity of PA-GFP-tubulin (bottom row) measured across the whole spindle (A) or along the gray line shown in inset (B). Vertical lines mark the signal intensity peaks; arrows show the separation of the photoactivated spots within the bridging fiber (A) and the distance between the photoactivated spots on the bridging and K-fiber (B).

(C) Box plot of velocities measured for parameters shown in the scheme. In the box plot, the central mark indicates the median, with the bottom and top edges of the box indicating the 25th and 75th percentiles, respectively. The whiskers extend to the most extreme data points, with exception of the outliers that are marked individually with the plus symbol.

(D) Correlation between velocities of sliding apart of bridging fibers and K-fibers; n, number of cells. Data were statistically analyzed using a t test (n.s., not significant). Scale bars, 1 μm. See also Figure S4.

(Figure 4D). By measuring the velocity of the photoactivated spots with respect to the spindle pole, we found that the bridging fiber and the attached K-fiber undergo poleward flux at a similar velocity (0.42 ± 0.06 μm/min and 0.32 ± 0.05 μm/min, respectively, n = 25, p = 0.19) (Figure 4C and Table 1). The flux velocity of the K-fibers is in agreement with previous indirect estimation of poleward flux velocity in anaphase (Ganem et al., 2005). Pac-Man depolymerization, measured as the velocity at which the kinetochore approached the photoactivated spot, occurred at the rate of 0.43 ± 0.13 μm/min (n = 20). During the same time period, the kinetochores segregated at a velocity of 2.76 ± 0.27 μm/min (n = 20, Figures 4C and S4A) and poleward kinetochore velocity was 0.75 ± 0.14 (sum of Pac-Man and poleward flux velocities shown above, n = 20). In addition, we found that the lengthening velocity of the contour consisting of the sister K-fibers and the bridging fiber (1.23 ± 0.17 μm/min, n = 20) was slower than the velocity of sliding of the bridging fibers itself, as expected in the presence of poleward flux (Figure 4C). In the same cells, spindle poles separated at a velocity of 1.36 ± 0.27 μm/min (n = 20, data not shown). Taken together, these results indicate that bridging fibers and K-fibers remain laterally linked and slide together during anaphase in intact spindles.

Theoretical Model for Kinetochore Separation

To explore whether kinetochore separation can be explained by sliding within the bridging fiber, which is laterally linked with K-fibers, we developed a one-dimensional theoretical model depicted in Figure 5A. In our model, movements of kinetochores, poles and laterally linked K-fibers and bridging fibers are calculated by the force-balance equations given in Figure 5B and STAR Methods.

For the initial values given in Figure 5A and the parameters in Figure 5B, numerical solutions of the model show separation of both kinetochore pairs in time (Figure 5C). Bridging MTs slide with respect to each other, with a velocity close to the motor sliding velocity without a load. K-fibers move with velocities similar to the velocities of the bridging fibers. Poles also separate, but slower than kinetochores and fibers (Figure 5C). Quantitative agreement with experimental velocities was obtained by a choice of free parameters, v_{k0}, v_{p0}, and v_m (Figure S5A and STAR Methods).

We aimed to compare our theory with the experiment of severing a K-fiber far away from the kinetochore. We modified our model by setting the forces at the pole in the upper right fibers to zero, $F^+_{pk} = F^+_{pb} = 0$, and describing the length of the right K-fiber, $x^+_{kf} - x^+_k$, at time $t = 0.5$ min. Numerical simulations show that kinetochores, bridging fibers, and K-fibers move with similar velocities irrespective of whether K-fibers do or do not interact with poles (dashed and solid lines in Figure 5D, respectively). These results are in agreement with the movement of displaced kinetochores observed in our experiments (Figure 1). To compare our theory with the experiment in which a K-fiber and

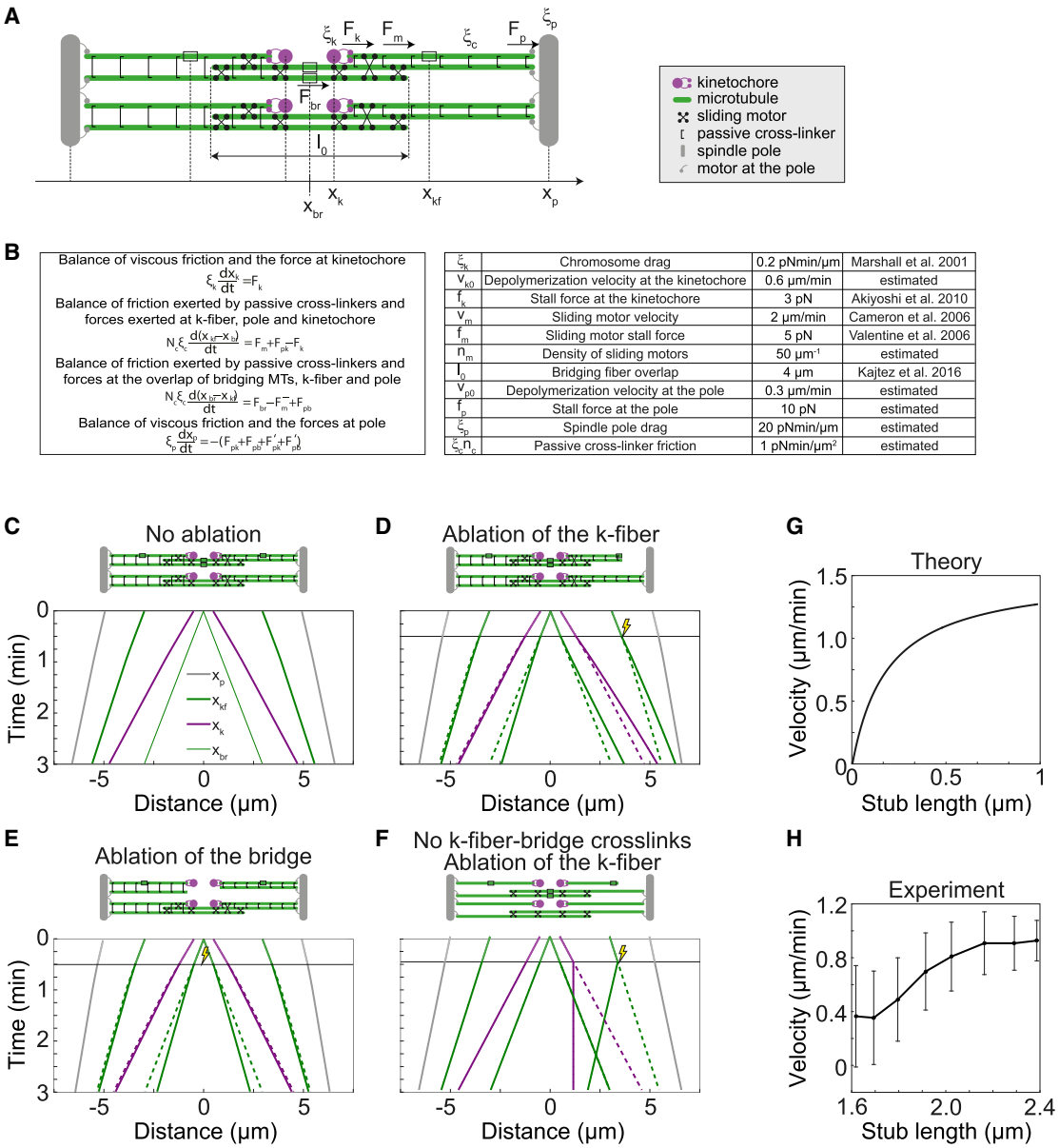

ξ_k	Chromosome drag	0.2 pNmin/μm	Marshall et al. 2001
v_{k0}	Depolymerization velocity at the kinetochore	0.6 μm/min	estimated
f_k	Stall force at the kinetochore	3 pN	Akiyoshi et al. 2010
v_m	Sliding motor velocity	2 μm/min	Cameron et al. 2006
f_m	Sliding motor stall force	5 pN	Valentine et al. 2006
n_m	Density of sliding motors	50 μm^{-1}	estimated
l_0	Bridging fiber overlap	4 μm	Kajtez et al. 2016
v_{p0}	Depolymerization velocity at the pole	0.3 μm/min	estimated
f_p	Stall force at the pole	10 pN	estimated
ξ_p	Spindle pole drag	20 pNmin/μm	estimated
$\xi_c n_c$	Passive cross-linker friction	1 pNmin/μm^2	estimated

Figure 5. The Theoretical Model of Anaphase

(A) Scheme of the model. Kinetochores (magenta) are initially (t = 0) positioned at the positions $x_k^{\pm} = \pm 0.5$ μm. K-fibers (green) extend from the kinetochores to spindle poles (gray) initially positioned at $x_p^{\pm} = \pm 5$ μm. Initial position of the K-fibers is $x_{kf}^{\pm} = \pm 3.0$ μm. Bridging fiber microtubules (green) extend from the central overlap of constant length l_0 toward poles. Initial position of the bridging fibers is $x_{br}^{\pm} = 0$. Molecular motors (cross signs) connect antiparallel MTs and generate sliding forces F_m and F_{br}. Passive crosslinkers (open bracket shape) connect parallel MTs and generate friction characterized by a friction coefficient ξ_c. Symbols F_k and F_p denote pulling forces generated at the kinetochores and at the poles, respectively. Symbols ξ_k and ξ_p denote friction coefficients of the kinetochores and the poles, respectively.

(B) Left: model equations for right half of the spindle. Superscripts + and − denote the right and left sides, respectively. Forces exerted by the second pair of K-fibers, and bridging MTs are calculated by adding a prime symbol to all variables. Right: parameters of the model. Five parameter values were taken from previous studies (Akiyoshi et al., 2010; Cameron et al., 2006; Kajtez et al., 2016; Marshall et al., 2001; Valentine et al., 2006), as indicated.

(C–F) Upper: scheme of the model. Lower: positions of kinetochores, K-fibers, bridging fibers, and spindle poles are shown as a function of time for the parameters given in (B). Solid and dashed lines correspond to the upper and lower fiber, respectively. (C) Solutions of model. (D) Solutions of the modified model in which the forces at the pole in the upper right fibers are set to zero at time t = 0.5 min. (E) Solutions of the modified model in which the forces between antiparallel MTs in the upper fiber are set to zero at time t = 0.5 min. (F) Solutions of the modified model without the connection between K-fibers and bridging fibers. In addition, the forces at the pole in the upper right fibers are set to zero at time t = 0.5 min.

(G) The velocity of the right kinetochore shown as function of the length of the fiber stub. Numerical results are obtained by parameters given in (B).

(H) Experimental measurement of the detached kinetochore-midpoint velocity dependence on the length of the K-fiber stub (n = 8 cells). Error bars represent SEM.

See also Figure S5.

the linked bridging fiber were severed, we additionally modified the model by setting the forces between antiparallel fibers to zero, $F_{br} = F_m^{\pm} = 0$. In this case, the right kinetochore does not move (Figure S5B). This behavior is in agreement with the double-ablation experiment (Figures 2A–2C).

To compare our theory with the experiment of severing the bridging fibers, we modified our model by setting the forces between antiparallel MTs in the upper fiber to zero, $F_{br} = F_m^{\pm} = 0$, at time $t = 0.5$ min. Numerical simulations show that the movement of kinetochores, bridging fibers, and K-fibers is similar to that in the unmodified model (Figures 5C and 5E). These results are in qualitative agreement with the poleward movement of kinetochores observed in our experiments in which the midzone was severed (Figures 2G–2I). However, the theory does not reproduce the pronounced experimentally observed slowdown of the pole separation, as expected, given that in the experiments most of the bridging fibers were severed whereas in the theory the forces in one out of two bridging fibers were set to zero.

In comparison with previous models for anaphase (Brust-Mascher et al., 2004; Civelekoglu-Scholey et al., 2006; Cytrynbaum et al., 2003; Wollman et al., 2008), the main new ingredient of our model is the connection between K-fibers and bridging fibers. To explore the relevance of this connection, we modified our model by setting the forces $F_m^{\pm} = 0$ and the number of passive crosslinkers $N_c^{\pm} = 0$. Numerical solutions of the modified model are similar to those of the original model (compare Figures 5C and S5C). However, the model without the connection between K-fibers and bridging fibers cannot explain the experimentally observed separation of kinetochores upon severance of a K-fiber, as shown in our simulation where we set the forces in the upper right fibers to zero, $F_{pk}^{+} = F_{pb}^{+} = 0$, at time $t = 0.5$ min (Figure 5F). Thus, the connection between K-fibers and bridging fibers is relevant to explain the kinetochore separation observed in our experiments.

Our model provides an independent prediction for the experiment of K-fiber severing. In our model, when we set the forces in the upper right fibers to zero (Figure 5D), the velocity of the right kinetochore increases with the length of the K-fiber stub, $x_{kf}^{+} - x_k^{+}$ (Figure 5G). To experimentally test this prediction, we used the data from the K-fiber severing experiments to measure the k fiber stub length and the kinetochore movement (Figures S5D and S5E). As predicted by the model, we found that the kinetochore velocity increases with the K-fiber stub length (Figure 5H). In the experiments, the velocity approaches zero for a finite stub length most likely because the K-fiber is not linked to the bridging fiber up to $\sim$1 μm from the kinetochore (Kajtez et al., 2016; Milas and Tolić, 2016), whereas this geometrical feature is not included in the model. Based on the results of our model and experiments, we conclude that sliding within the bridging fiber, which is laterally linked with K-fibers along their length, pushes K-fibers poleward by the friction of passive crosslinks between these fibers.

DISCUSSION

Our work revealed that the pushing forces exerted by the bridging fiber are able to segregate chromosomes independently of the spindle pole. This result is unexpected because according to the current view, the processes that contribute to kinetochore separation require kinetochores to be linked, directly or indirectly, with the spindle pole. Pioneering micromanipulation experiments (Nicklas et al., 1982, 1989) in cricket and grasshopper spindles where a centrosome was removed have shown that chromosomes continue to move poleward in anaphase as long as the K-fiber stub is longer than 1 μm (Nicklas, 1989). However, in these experiments K-fibers remained focused into a pole, and thus the role of kinetochore-pole connections remained unexplored. Recent studies have shown that direct kinetochore-pole connections are not required for chromosome segregation in mammalian cells, because short K-fibers can move chromosomes poleward through interactions with adjacent spindle MTs (Elting et al., 2014; Sikirzhytski et al., 2014). On the contrary, in our study the K-fiber stub was oriented away from the entire spindle and the kinetochore attached to the stub moved away from the pole to which it was originally connected. Thus, the kinetochores segregated without any connection, direct or indirect, to one spindle pole.

Similar experiments in which centrosomes in *Caenorhabditis elegans* were destroyed by laser ablation showed that chromosomes can segregate without centrosomes, most likely by outward forces generated by midzone MTs that push against chromosomes (Nahaboo et al., 2015). This model differs from ours, where the bridging MTs push the K-fibers apart rather than pushing directly on the chromosomes.

Transport of chromosomes toward the spindle poles is facilitated by shortening of K-fibers through Pac-Man and poleward flux mechanisms. Our work provides the first direct measurements of the contributions of Pac-Man and poleward flux to the poleward kinetochore velocity in human cells, which are 60% and 40%, respectively. These contributions are similar to those in *Drosophila* S2 cells (Matos et al., 2009), but different to those in *Xenopus* egg extracts where poleward flux dominates (Desai et al., 1998), and in fission yeast where poleward flux does not occur (Mallavarapu et al., 1999). Moreover, the flux velocities measured here are in qualitative agreement with previous results for K-fibers in newt lung cells (Mitchison and Salmon, 1992) and for interpolar MTs in PtK1 cells (Saxton and McIntosh, 1987).

Our measurements show that anaphase B spindle elongation, driven by MT sliding, and anaphase A poleward kinetochore movement contribute roughly equally to kinetochore segregation. The experiments in which the midzone was severed show that interpolar fibers are required for proper spindle pole separation, whereas the contribution of cortical pulling forces is not significant. This is similar to pole-pole separation by outward sliding of interpolar MTs in diatoms, fission yeast, grasshopper, and *Drosophila* embryo (Brust-Mascher et al., 2009; Khodjakov et al., 2004; Leslie and Pickett-Heaps, 1983; Tolic-Norrelykke et al., 2004). Our results support a view that the pushing forces from the midzone interpolar fibers, combined with the regulation of MT dynamics at the kinetochore and the pole, define the speed of chromosome and centrosome separation in human cells, as previously discussed (Betterton and McIntosh, 2013). On the contrary, severance of the spindle midzone accelerated pole separation during anaphase B in *Nectria haematococca*, PtK2 cells, and *C. elegans* (Aist et al., 1991, 1993; Grill et al., 2001). These experiments, together with results from Eg5 inhibition (Collins et al., 2014), suggest that, in some model systems,

midzone microtubules serve as a brake on pole-to-pole separation. In addition, disruption of astral MTs in our experiments did not affect spindle pole separation, which is contrary to the previous experiments demonstrating a contribution from cortical pulling on spindle pole separation in PtK2 cells (Aist et al., 1993). Such differences could be a consequence of versatility of anaphase mechanisms in different model systems. Moreover, anaphase relies on multiple mechanisms even within the same model organism (Maiato and Lince-Faria, 2010; Scholey et al., 2016).

The contribution of motor proteins to sliding of antiparallel MTs in anaphase of human cells is largely unknown (Maiato and Lince-Faria, 2010). Our experiments suggest that MKLP1 contributes to chromosome and pole separation. We show that MKLP1 affects the stability of midzone microtubules in early stages of anaphase, which was previously observed in cytokinesis (Glotzer, 2009). Thus, we speculate that this protein takes part in bundling and possibly also sliding of antiparallel MTs in early anaphase, similarly to its role in anaphase B in fission yeast (Fu et al., 2009). This is in agreement with previous work showing that the centralspindlin complex influences midzone elongation during cytokinesis in human cells (Hu et al., 2011).

Inhibition of Eg5, the motor that drives spindle elongation in yeast (Khmelinskii et al., 2009), *Xenopus* (Shirasu-Hiza et al., 2004), and *Drosophila* (Brust-Mascher et al., 2009), did not affect sliding rates in anaphase in our experiments. This result is consistent with the previous observations that this motor had no effect on midzone elongation in HeLa cells (Hu et al., 2011), but different from the observed accelerated spindle elongation in STLC-treated LLC-Pk1 cells (Collins et al., 2014). Depletion of KIF15 alone or together with inhibition of Eg5 did not affect MT sliding in early anaphase, although it was previously shown that Eg5 and KIF15 cooperate in outward force generation during preanaphase stages of mitosis (Tanenbaum et al., 2009; van Heesbeen et al., 2014). However, recent work suggests that KIF15 crosslinks mainly parallel MTs (Drechsler and McAinsh, 2016), making it a less likely candidate for antiparallel sliding.

Along with the motor proteins, our theory relies on a connection between the bridging fiber and K-fibers, which is established by parallel non-motor crosslinkers. It was shown that parallel crosslinkers called "the mesh" connect MTs in a K-fiber (Nixon et al., 2015). However, these proteins could also crosslink K-fiber MTs and bridging MTs in the regions of their parallel overlap. The exact position of the minus ends of the bridging MTs, and the nature of their interaction with K-fibers in regions of parallel overlap, is yet to be elucidated. The antiparallel overlaps contain the crosslinker PRC1 (Kajtez et al., 2016; Polak et al., 2017), which, together with the parallel crosslinkers, will be an important subject for future studies since their roles in anaphase are largely unknown.

Our experiments and theory revisit the old ideas that force for anaphase movement can be generated in the midzone (Belar, 1929) by MT sliding and pushing, and transmitted along the entire K-fiber. Östergren (1951) proposed that these forces are produced all along the K-fiber rather than only at its ends. McIntosh et al. (1969) suggested that MT sliding moves the chromosomes. Crosslinking between K-fibers and interpolar MTs in anaphase has been discussed in several works (Goode, 1981; Maiato and Lince-Faria, 2010; Margolis et al., 1978; Matos et al., 2009; Mitchison, 2005); however, these ideas have not been directly tested and remain largely unappreciated. Our work revisits the concept of forces resulting from crosslinking K-fiber and non-K-fiber MTs, demonstrating that these forces work together with the forces generated by K-fiber shortening to segregate chromosomes in human cells.

STAR★METHODS

Detailed methods are provided in the online version of this paper and include the following:

- KEY RESOURCES TABLE
- CONTACT FOR REAGENT AND RESOURCE SHARING
- EXPERIMENTAL MODEL AND SUBJECT DETAILS
  - Cell Lines
- METHOD DETAILS
  - Sample Preparation
  - Imaging Combined with Laser Ablation
  - Imaging Combined with Photoactivation
  - Transfection
  - Immunostaining
  - Protein Depletion and Inactivation Experiments
  - Theory
  - Choice of Parameter Values
- QUANTIFICATION AND STATISTICAL ANALYSIS

SUPPLEMENTAL INFORMATION

Supplemental Information includes five figures and three movies and can be found with this article online at https://doi.org/10.1016/j.devcel.2017.09.010.

AUTHOR CONTRIBUTIONS

K.V. and R.B. carried out and analyzed all experiments, except photoactivation on intact spindles, which was done by A.M. A.B. developed the theoretical model. I.M.T. and N.P. conceived the project and supervised experiments and theory, respectively. All authors wrote the paper.

ACKNOWLEDGMENTS

We thank Helder Maiato and Marin Barišić for the U2OS cell line; Jan Peychl and Sebastian Bundschuh from the Light Microscopy Facility of Max Planck Institute of Molecular Cell Biology and Genetics in Dresden; Marc Koch, Alberto Zorloni, and Igor Weber and his group for support with microscopy systems; Tony Hyman's group for help with cell culture; Heike Petzold for assistance; the entire I.M.T. and N.P. groups for discussions and for constructive comments on the manuscript; and Ivana Šarić for the drawings. A.B. acknowledges the support of the German Research Foundation (DFG, GZ: TO 564/7-1). This work was funded by the European Research Council (ERC, GA number 647077).

Received: February 14, 2017
Revised: July 21, 2017
Accepted: September 13, 2017
Published: October 9, 2017

REFERENCES

Aist, J.R., Bayles, C.J., Tao, W., and Berns, M.W. (1991). Direct experimental evidence for the existence, structural basis and function of astral forces during anaphase B in vivo. J. Cell Sci. *100* (Pt 2), 279–288.

Aist, J.R., Liang, H., and Berns, M.W. (1993). Astral and spindle forces in PtK2 cells during anaphase B: a laser microbeam study. J. Cell Sci. *104* (Pt 4), 1207–1216.

Akiyoshi, B., Sarangapani, K.K., Powers, A.F., Nelson, C.R., Reichow, S.L., Arellano-Santoyo, H., Gonen, T., Ranish, J.A., Asbury, C.L., and Biggins, S. (2010). Tension directly stabilizes reconstituted kinetochore-microtubule attachments. Nature *468*, 576–579.

Asbury, C.L. (2017). Anaphase A: disassembling microtubules move chromosomes toward spindle poles. Biology (Basel) *6*, http://dx.doi.org/10.3390/biology6010015.

Barisic, M., Aguiar, P., Geley, S., and Maiato, H. (2014). Kinetochore motors drive congression of peripheral polar chromosomes by overcoming random arm-ejection forces. Nat. Cell Biol. *16*, 1249–1256.

Belar, K. (1929). Beiträge zur Kausalanalyse der Mitose. Wilhelm Roux Arch. Entwickl Mech. Org. *118*, 359–484.

Betterton, M.D., and McIntosh, J.R. (2013). Regulation of chromosome speeds in mitosis. Cell. Mol. Bioeng. *6*, 418–430.

Blangy, A., Lane, H.A., d'Herin, P., Harper, M., Kress, M., and Nigg, E.A. (1995). Phosphorylation by p34cdc2 regulates spindle association of human Eg5, a kinesin-related motor essential for bipolar spindle formation in vivo. Cell *83*, 1159–1169.

Brust-Mascher, I., Civelekoglu-Scholey, G., Kwon, M., Mogilner, A., and Scholey, J.M. (2004). Model for anaphase B: role of three mitotic motors in a switch from poleward flux to spindle elongation. Proc. Natl. Acad. Sci. USA *101*, 15938–15943.

Brust-Mascher, I., Sommi, P., Cheerambathur, D.K., and Scholey, J.M. (2009). Kinesin-5-dependent poleward flux and spindle length control in *Drosophila* embryo mitosis. Mol. Biol. Cell *20*, 1749–1762.

Buda, R., Vukusic, K., and Tolic, I.M. (2017). Dissection and characterization of microtubule bundles in the mitotic spindle using femtosecond laser ablation. Methods Cell Biol. *139*, 81–101.

Cameron, L.A., Yang, G., Cimini, D., Canman, J.C., Kisurina-Evgenieva, O., Khodjakov, A., Danuser, G., and Salmon, E.D. (2006). Kinesin 5-independent poleward flux of kinetochore microtubules in PtK1 cells. J. Cell Biol. *173*, 173–179.

Civelekoglu-Scholey, G., Sharp, D.J., Mogilner, A., and Scholey, J.M. (2006). Model of chromosome motility in *Drosophila* embryos: adaptation of a general mechanism for rapid mitosis. Biophys. J. *90*, 3966–3982.

Collins, E., Mann, B.J., and Wadsworth, P. (2014). Eg5 restricts anaphase B spindle elongation in mammalian cells. Cytoskeleton (Hoboken) *71*, 136–144.

Cytrynbaum, E.N., Scholey, J.M., and Mogilner, A. (2003). A force balance model of early spindle pole separation in *Drosophila* embryos. Biophys. J. *84*, 757–769.

Desai, A., Maddox, P.S., Mitchison, T.J., and Salmon, E.D. (1998). Anaphase A chromosome movement and poleward spindle microtubule flux occur at similar rates in *Xenopus* extract spindles. J. Cell Biol. *141*, 703–713.

Drechsler, H., and McAinsh, A.D. (2016). Kinesin-12 motors cooperate to suppress microtubule catastrophes and drive the formation of parallel microtubule bundles. Proc. Natl. Acad. Sci. USA *113*, E1635–E1644.

Elting, M.W., Hueschen, C.L., Udy, D.B., and Dumont, S. (2014). Force on spindle microtubule minus ends moves chromosomes. J. Cell Biol. *206*, 245–256.

Fontijn, R.D., Goud, B., Echard, A., Jollivet, F., van Marle, J., Pannekoek, H., and Horrevoets, A.J. (2001). The human kinesin-like protein RB6K is under tight cell cycle control and is essential for cytokinesis. Mol. Cell. Biol. *21*, 2944–2955.

Fu, C., Ward, J.J., Loiodice, I., Velve-Casquillas, G., Nedelec, F.J., and Tran, P.T. (2009). Phospho-regulated interaction between kinesin-6 Klp9p and microtubule bundler Ase1p promotes spindle elongation. Dev. Cell *17*, 257–267.

Ganem, N.J., Upton, K., and Compton, D.A. (2005). Efficient mitosis in human cells lacking poleward microtubule flux. Curr. Biol. *15*, 1827–1832.

Glotzer, M. (2009). The 3Ms of central spindle assembly: microtubules, motors and MAPs. Nat. Rev. Mol. Cell Biol. *10*, 9–20.

Goode, D. (1981). Microtubule turnover as a mechanism of mitosis and its possible evolution. Biosystems *14*, 271–287.

Gorbsky, G.J., Sammak, P.J., and Borisy, G.G. (1987). Chromosomes move poleward in anaphase along stationary microtubules that coordinately disassemble from their kinetochore ends. J. Cell Biol. *104*, 9–18.

Grill, S.W., Gonczy, P., Stelzer, E.H., and Hyman, A.A. (2001). Polarity controls forces governing asymmetric spindle positioning in the *Caenorhabditis elegans* embryo. Nature *409*, 630–633.

Hiramoto, Y., and Nakano, Y. (1988). Micromanipulation studies of the mitotic apparatus in sand dollar eggs. Cell Motil. Cytoskeleton *10*, 172–184.

Hu, C.K., Coughlin, M., Field, C.M., and Mitchison, T.J. (2011). KIF4 regulates midzone length during cytokinesis. Curr. Biol. *21*, 815–824.

Jiang, W., Jimenez, G., Wells, N.J., Hope, T.J., Wahl, G.M., Hunter, T., and Fukunaga, R. (1998). PRC1: a human mitotic spindle-associated CDK substrate protein required for cytokinesis. Mol. Cell *2*, 877–885.

Kajtez, J., Solomatina, A., Novak, M., Polak, B., Vukusic, K., Rudiger, J., Cojoc, G., Milas, A., Sumanovac Sestak, I., Risteski, P., et al. (2016). Overlap microtubules link sister k-fibres and balance the forces on bi-oriented kinetochores. Nat. Commun. *7*, 10298.

Kapitein, L.C., Peterman, E.J., Kwok, B.H., Kim, J.H., Kapoor, T.M., and Schmidt, C.F. (2005). The bipolar mitotic kinesin Eg5 moves on both microtubules that it crosslinks. Nature *435*, 114–118.

Khmelinskii, A., Roostalu, J., Roque, H., Antony, C., and Schiebel, E. (2009). Phosphorylation-dependent protein interactions at the spindle midzone mediate cell cycle regulation of spindle elongation. Dev. Cell *17*, 244–256.

Khodjakov, A., La Terra, S., and Chang, F. (2004). Laser microsurgery in fission yeast; role of the mitotic spindle midzone in anaphase B. Curr. Biol. *14*, 1330–1340.

Krull, A., Steinborn, A., Ananthanarayanan, V., Ramunno-Johnson, D., Petersohn, U., and Tolic-Norrelykke, I.M. (2014). A divide and conquer strategy for the maximum likelihood localization of low intensity objects. Opt. Express *22*, 210–228.

Leslie, R.J., and Pickett-Heaps, J.D. (1983). Ultraviolet microbeam irradiations of mitotic diatoms: investigation of spindle elongation. J. Cell Biol. *96*, 548–561.

Lukinavicius, G., Reymond, L., D'Este, E., Masharina, A., Gottfert, F., Ta, H., Guther, A., Fournier, M., Rizzo, S., Waldmann, H., et al. (2014). Fluorogenic probes for live-cell imaging of the cytoskeleton. Nat. Methods *11*, 731–733.

Maiato, H., and Lince-Faria, M. (2010). The perpetual movements of anaphase. Cell. Mol. Life Sci. *67*, 2251–2269.

Mallavarapu, A., Sawin, K., and Mitchison, T. (1999). A switch in microtubule dynamics at the onset of anaphase B in the mitotic spindle of *Schizosaccharomyces pombe*. Curr. Biol. *9*, 1423–1426.

Margolis, R.L., Wilson, L., and Keifer, B.I. (1978). Mitotic mechanism based on intrinsic microtubule behaviour. Nature *272*, 450–452.

Marshall, W.F., Marko, J.F., Agard, D.A., and Sedat, J.W. (2001). Chromosome elasticity and mitotic polar ejection force measured in living *Drosophila* embryos by four-dimensional microscopy-based motion analysis. Curr. Biol. *11*, 569–578.

Mastronarde, D.N., McDonald, K.L., Ding, R., and McIntosh, J.R. (1993). Interpolar spindle microtubules in PTK cells. J. Cell Biol. *123*, 1475–1489.

Matos, I., Pereira, A.J., Lince-Faria, M., Cameron, L.A., Salmon, E.D., and Maiato, H. (2009). Synchronizing chromosome segregation by flux-dependent force equalization at kinetochores. J. Cell Biol. *186*, 11–26.

McDonald, K.L., O'Toole, E.T., Mastronarde, D.N., and McIntosh, J.R. (1992). Kinetochore microtubules in PTK cells. J. Cell Biol. *118*, 369–383.

McIntosh, J.R., Hepler, P.K., and Van Wie, D.G. (1969). Model for mitosis. Nature *224*, 659–663.

McIntosh, J.R., and Landis, S.C. (1971). The distribution of spindle microtubules during mitosis in cultured human cells. J. Cell Biol. *49*, 468–497.

McIntosh, J.R., Molodtsov, M.I., and Ataullakhanov, F.I. (2012). Biophysics of mitosis. Q. Rev. Biophys. *45*, 147–207.

Milas, A., and Tolić, I.M. (2016). Relaxation of interkinetochore tension after severing of a k-fiber depends on the length of the k-fiber stub. Matters (Zür). http://dx.doi.org/10.19185/matters.201603000025.

Mishima, M., Kaitna, S., and Glotzer, M. (2002). Central spindle assembly and cytokinesis require a kinesin-like protein/RhoGAP complex with microtubule bundling activity. Dev. Cell *2*, 41–54.

Mitchison, T., Evans, L., Schulze, E., and Kirschner, M. (1986). Sites of microtubule assembly and disassembly in the mitotic spindle. Cell *45*, 515–527.

Mitchison, T.J. (1989). Polewards microtubule flux in the mitotic spindle: evidence from photoactivation of fluorescence. J. Cell Biol. *109*, 637–652.

Mitchison, T.J. (2005). Mechanism and function of poleward flux in *Xenopus* extract meiotic spindles. Philos. Trans. R. Soc. Lond. B Biol. Sci. *360*, 623–629.

Mitchison, T.J., and Salmon, E.D. (1992). Poleward kinetochore fiber movement occurs during both metaphase and anaphase-A in newt lung cell mitosis. J. Cell Biol. *119*, 569–582.

Mollinari, C., Kleman, J.-P., Jiang, W., Schoehn, G., Hunter, T., and Margolis, R.L. (2002). PRC1 is a microtubule binding and bundling protein essential to maintain the mitotic spindle midzone. J. Cell Biol. *157*, 1175–1186.

Nahaboo, W., Zouak, M., Askjaer, P., and Delattre, M. (2015). Chromatids segregate without centrosomes during *Caenorhabditis elegans* mitosis in a Ran- and CLASP-dependent manner. Mol. Biol. Cell *26*, 2020–2029.

Nicklas, R.B. (1989). The motor for poleward chromosome movement in anaphase is in or near the kinetochore. J. Cell Biol. *109*, 2245–2255.

Nicklas, R.B., Kubai, D.F., and Hays, T.S. (1982). Spindle microtubules and their mechanical associations after micromanipulation in anaphase. J. Cell Biol. *95*, 91–104.

Nicklas, R.B., Lee, G.M., Rieder, C.L., and Rupp, G. (1989). Mechanically cut mitotic spindles: clean cuts and stable microtubules. J. Cell Sci. *94* (Pt 3), 415–423.

Nislow, C., Lombillo, V.A., Kuriyama, R., and McIntosh, J.R. (1992). A plus-end-directed motor enzyme that moves antiparallel microtubules in vitro localizes to the interzone of mitotic spindles. Nature *359*, 543–547.

Nixon, F.M., Gutierrez-Caballero, C., Hood, F.E., Booth, D.G., Prior, I.A., and Royle, S.J. (2015). The mesh is a network of microtubule connectors that stabilizes individual kinetochore fibers of the mitotic spindle. Elife *4*, e07635.

Nixon, F.M., Honnor, T.R., Clarke, N.I., Starling, G.P., Beckett, A.J., Johansen, A.M., Brettschneider, J.A., Prior, I.A., and Royle, S.J. (2017). Microtubule organization within mitotic spindles revealed by serial block face scanning electron microscopy and image analysis. J. Cell Sci. *130*, 1845–1855.

Östergren, G. (1951). The mechanism of co-orientation in bivalents and multivalents. Hereditas *37*, 85–156.

Pavin, N., and Tolic, I.M. (2016). Self-organization and forces in the mitotic spindle. Annu. Rev. Biophys. *45*, 279–298.

Polak, B., Risteski, P., Lesjak, S., and Tolic, I.M. (2017). PRC1-labeled microtubule bundles and kinetochore pairs show one-to-one association in metaphase. EMBO Rep. *18*, 217–230.

Sawin, K.E., LeGuellec, K., Philippe, M., and Mitchison, T.J. (1992). Mitotic spindle organization by a plus-end-directed microtubule motor. Nature *359*, 540–543.

Saxton, W.M., and McIntosh, J.R. (1987). Interzone microtubule behavior in late anaphase and telophase spindles. J. Cell Biol. *105*, 875–886.

Schneider, C.A., Rasband, W.S., and Eliceiri, K.W. (2012). NIH Image to ImageJ: 25 years of image analysis. Nat. Methods *9*, 671–675.

Scholey, J.M., Civelekoglu-Scholey, G., and Brust-Mascher, I. (2016). Anaphase B. Biology (Basel) *5*, http://dx.doi.org/10.3390/biology5040051.

Shirasu-Hiza, M., Perlman, Z.E., Wittmann, T., Karsenti, E., and Mitchison, T.J. (2004). Eg5 causes elongation of meiotic spindles when flux-associated microtubule depolymerization is blocked. Curr. Biol. *14*, 1941–1945.

Sikirzhytski, V., Magidson, V., Steinman, J.B., He, J., Le Berre, M., Tikhonenko, I., Ault, J.G., McEwen, B.F., Chen, J.K., Sui, H., et al. (2014). Direct kinetochore-spindle pole connections are not required for chromosome segregation. J. Cell Biol. *206*, 231–243.

Skoufias, D.A., DeBonis, S., Saoudi, Y., Lebeau, L., Crevel, I., Cross, R., Wade, R.H., Hackney, D., and Kozielski, F. (2006). S-trityl-L-cysteine is a reversible, tight binding inhibitor of the human kinesin Eg5 that specifically blocks mitotic progression. J. Biol. Chem. *281*, 17559–17569.

Stumpff, J., von Dassow, G., Wagenbach, M., Asbury, C., and Wordeman, L. (2008). The kinesin-8 motor Kif18A suppresses kinetochore movements to control mitotic chromosome alignment. Dev. Cell *14*, 252–262.

Tanenbaum, M.E., Macurek, L., Janssen, A., Geers, E.F., Alvarez-Fernandez, M., and Medema, R.H. (2009). Kif15 cooperates with eg5 to promote bipolar spindle assembly. Curr. Biol. *19*, 1703–1711.

Tolić, I.M. (2017). Mitotic spindle: kinetochore fibers hold on tight to interpolar bundles. Eur. Biophys. J. http://dx.doi.org/10.1007/s00249-017-1244-4.

Tolic, I.M., and Pavin, N. (2016). Bridging the gap between sister kinetochores. Cell Cycle *15*, 1169–1170.

Tolic-Norrelykke, I.M., Sacconi, L., Thon, G., and Pavone, F.S. (2004). Positioning and elongation of the fission yeast spindle by microtubule-based pushing. Curr. Biol. *14*, 1181–1186.

Valentine, M.T., Fordyce, P.M., Krzysiak, T.C., Gilbert, S.P., and Block, S.M. (2006). Individual dimers of the mitotic kinesin motor Eg5 step processively and support substantial loads in vitro. Nat. Cell Biol. *8*, 470–476.

van Beuningen, S.F., Will, L., Harterink, M., Chazeau, A., van Battum, E.Y., Frias, C.P., Franker, M.A., Katrukha, E.A., Stucchi, R., Vocking, K., et al. (2015). TRIM46 controls neuronal polarity and axon specification by driving the formation of parallel microtubule arrays. Neuron *88*, 1208–1226.

van Heesbeen, R.G., Tanenbaum, M.E., and Medema, R.H. (2014). Balanced activity of three mitotic motors is required for bipolar spindle assembly and chromosome segregation. Cell Rep. *8*, 948–956.

Vanneste, D., Takagi, M., Imamoto, N., and Vernos, I. (2009). The role of Hklp2 in the stabilization and maintenance of spindle bipolarity. Curr. Biol. *19*, 1712–1717.

Wollman, R., Civelekoglu-Scholey, G., Scholey, J.M., and Mogilner, A. (2008). Reverse engineering of force integration during mitosis in the Drosophila embryo. Mol. Syst. Biol. *4*, 195.

Yang, Z., Tulu, U.S., Wadsworth, P., and Rieder, C.L. (2007). Kinetochore dynein is required for chromosome motion and congression independent of the spindle checkpoint. Curr. Biol. *17*, 973–980.

STAR★METHODS

KEY RESOURCES TABLE

REAGENT or RESOURCE	SOURCE	IDENTIFIER
Antibodies		
α-tubulin rabbit polyclonal	Sigma-Aldrich	Cat# SAB4500087; RRID: AB_10743646
Alexa 405 conjugated donkey anti-rabbit IgG	Abcam	Cat# ab175649; RRID: AB_2715515
Chemicals, Peptides, and Recombinant Proteins		
Dulbecco's Modified Eagle's medium (DMEM)	Lonza	Cat# BE12-604F/U1
Fetal Bovine Serum (FBS)	Sigma-Aldrich	Cat# F2442
Geneticin	Life Technologies	Cat# 11811031
Penicillin/streptomycin solution	Lonza	Cat# DE17-502E
Trypsin/EDTA solution	Biochrom	Cat# L 2153
Leibovit's (L-15) CO2-independent medium	Life-Technologies	Cat# 21083027
Normal goat serum (NGS)	EMD Milipore Corp.	Cat# 566380-10ML
Opti-MEM medium	Life Technologies	Cat# 31985070
Lipofectamine RNAiMAX Reagent	Life Technologies	Cat# 13778150
(+)_S-Trityl-L-cysteine (STLC)	Sigma-Aldrich	Cat# 164739
Critical Commercial Assays		
Amaxa Cell Line Nucleofactor Kit	Lonza	Cat# VCA-1001
SiR-tubulin Kit	Cytoskeleton Inc.	Cat# CY-SC002
Experimental Models: Cell Lines		
Human: U2OS cells	Barisic et al., 2014	N/A
Oligonucleotides		
MKLP-1 siRNA	Santa Cruz Biotechnology	Cat# sc-35936
KIF15 siRNA	Santa Cruz Biotechnology	Cat# sc-78517
Control siRNA-A	Santa Cruz Biotechnology	Cat# sc- 37007
Recombinant DNA		
mCherry-PRC1	van Beuningen et al., 2015	N/A
Software and Algorithms		
ImageJ	Schneider et al., 2012	https://imagej.net/NIH_Image
PrairieView	Bruker	N/A
MatLab R2015a	MathWorks	N/A
SciDavis	Free Software Foundation	http://scidavis.sourceforge.net
Low Light Tracking Tool (LLTT) - ImageJ plugin	Krull et al., 2014	http://imagej.net/Low_Light_Tracking_Tool

CONTACT FOR REAGENT AND RESOURCE SHARING

Further information and requests for reagents should be directed to and will be fulfilled by the Lead Contact, Iva M. Tolić (tolic@irb.hr).

EXPERIMENTAL MODEL AND SUBJECT DETAILS

Cell Lines

The cell line used is human U2OS (human osteosarcoma, female) permanently transfected and stabilized using CENP-A-GFP (protein of kinetochore complex), mCherry-α-tubulin, photoactivatable (PA)-GFP-tubulin, which was a gift from Marin Barišić and Helder Maiato (Institute for Molecular Cell Biology, University of Porto, Portugal). In experiments with transient expression of mCherry-PRC1 and live-cell staining with silicon rhodamine (SiR)-tubulin (Lukinavicius et al., 2014), we used a U2OS cell line stably expressing only CENP-A-GFP, which was a gift from the same group. Cells were grown in flasks in Dulbecco's Modified Eagle's medium (DMEM) (1 g/l D-glucose, L-glutamine, pyruvate) (Lonza, Basel, Switzerland) supplemented with 10% of heat-inactivated

Fetal Bovine Serum (FBS) (Sigma-Aldrich, St Louis, MO, USA), 50 μg/ml geneticin (Life Technologies, Waltham, MA, USA) and penicillin/streptomycin solution (Lonza) to a final concentration of 100 I.U./mL penicillin and 100 μg/mL streptomycin. The cells were kept at 37°C and 5% CO_2 in a Galaxy 170s humidified incubator (Eppendorf, Hamburg, Germany).

METHOD DETAILS

Sample Preparation

When cells reached 80% confluence, DMEM medium was removed from the flask and the cells were washed with 5 mL of 1% PBS. Afterward, 1 mL of 1% Trypsin/EDTA (Biochrom AG, Berlin, Germany) was added and the cells were incubated at 37°C and 5% CO2 in a humidified incubator (Eppendorf). After 5 min incubation, Trypsin was blocked by adding 5 mL of DMEM medium. Cells were counted using the Improved Neubauer chamber (BRAND GMBH + CO KG, Wertheim, Germany) and $4.5x10^5$ cells were seeded and cultured in 2 ml DMEM medium with same supplements (as above) at 37°C and 5% CO_2 on 35 mm glass coverslip uncoated dishes with 0.17mm (#1.5 coverglass) glass thickness (MatTek Corporation, Ashland, MA, USA). After one-day growth, 3h prior to imaging, the medium was replaced with Leibovit's (L-15) CO2-independent medium (Life Technologies), supplemented with 10% FBS (Life Technologies), 100 I.U./mL penicillin and 100 μg/mL streptomycin. For live-cell staining SiR-tubulin (Cytoskeleton Inc., Denver, CO, USA) was added to 1 mL of cells in a DMEM medium to a final concentration of 100 nM 5h before imaging together with efflux pump inhibitor verapamil (Cytoskeleton Inc.) to a final concentration of 10 μM.

Imaging Combined with Laser Ablation

U2OS cells were imaged using Bruker Opterra Multipoint Scanning Confocal Microscope (Bruker Nano Surfaces, Middleton, WI, USA). The system was mounted on a Nikon Ti-E inverted microscope equipped with a Nikon CFI Plan Apo VC 100x/1.4 numerical aperture oil objective (Nikon, Tokyo, Japan). The system was controlled with the Prairie View Imaging Software (Bruker). During imaging, cells were maintained at 37°C in Okolab Cage Incubator (Okolab, Pozzuoli, NA, Italy). In order to obtain the optimal balance between spatial resolution and signal-to-noise ratio, 60 μm pinhole aperture was used. For excitation of GFP and mCherry fluorescence, a 488 and a 561 nm diode laser line were used, respectively. The excitation light was separated from the emitted fluorescence by using Opterra Dichroic and Barrier Filter Set 405/488/561/640. Images were captured with an Evolve 512 Delta EMCCD Camera (Photometrics, Tucson, AZ, USA) using 150-300 ms exposure times. Electron multiplying gain was set on 300-500. Camera readout mode was 20 Mhz. No binning was performed. To bring the xy-pixel size in the image down to 83 nm, a 2x relay lens was placed in front of the camera. Z-stacks were acquired comprising 8-13 focal planes at a 0.5 μm z-spacing using 2xframe averaging. The z-scan mode was unidirectional. Image acquisition was performed for 20-40 time frames at 15-20 s intervals. Severing of microtubule bundles was performed during live imaging using a Mikan femtosecond laser oscillator (Amplitude Systemes, Pessac, France), which was coupled to the photoactivation module of the microscope, at a wavelength of 1030 nm. The laser power was set to 70-100% which corresponds to $\sim$ 0.7-1W power at the sample plane.

For cutting of K-fibers, the size of the region for ablation was 700-1000 nm and laser exposure time was 800-1000 ms. Laser ablation was performed during the second time frame from start of the imaging in z plane(s) in which a single MT bundle could be discerned. The cut was performed on one of the outermost K-fibers, in one set of experiments 2.5 μm and in the other 1 μm from the kinetochore. Due to the fast reattachment of the ablated K-fibers to neighboring MTs in U2OS cells, multiple sequential cuts were sometimes necessary. For cutting of bridging fibers, the size of the region for ablation was 700-1000 nm and laser exposure time was 800-1000 ms. Laser ablation was performed during the third time frame from the anaphase start in z plane(s) in which a MT bundle could be discerned. For midzone and astral MTs cutting experiments, the single point mode with the fixed size of a region for ablation at 500 nm was used, while the laser exposure time was controlled by holding the mouse button. In both experiments, the laser ablation was performed continuously through all imaged z-planes (10-12 z-planes at 0.5 μm spacing). For photoactivation of fluorescence of PA-GFP after ablation, a 405-nm laser diode (Coherent, Santa Clara, CA, USA) was used. Photoactivation was performed using photoactivation option in software, with duration of pulse set to 80 ms. Further details of this microscopy system and similar laser ablation assays were discussed elsewhere (Buda et al., 2017).

U2OS cells in experiment where the cut was performed 2.5 μm from the kinetochore (Figures 1 and S1) were imaged by using a Zeiss LSM 710 NLO inverted laser scanning microscope with a Zeiss PlanApo X 63/1.4 oil immersion objective (Zeiss, Jena, Germany) heated with an objective heater system (Bioptechs, Butler, PA, USA). During imaging, cells were maintained at 37°C in Tempcontrol 37-2 digital Bachhoffer chamber (Zeiss). For excitation, a 488-nm line of a multiline Argon-Ion laser (0.45 mW; LASOS, Jena, Germany) and helium-neon (HeNe) 594 nm laser (0.11 mW) were used for GFP and RFP/mCherry, respectively. Spectral array detector from 34-Channel QUASAR Detection Unit (Zeiss) was used for detection of fluorescent light. Emission wavelengths for simultaneous image acquisition were selected by the sliding prisms incorporated in the detection unit. GFP and RFP/mCherry emissions were detected in ranges of 490–561 and 597–695 nm, respectively. No images were acquired during laser ablation. *xy* pixel size was set to 81 nm. Pinhole diameter was set to 0.7 μm (1 arbitrary unit). Pixel dwell time was 1 μs. Z-stacks were acquired at six focal planes with 0.5 μm spacing. The thickness of the optical sections was 700 nm. Image acquisition was performed for 20–40 time frames with 3.5–4.5 s intervals using unidirectional scanning. A titanium-sapphire (Ti:Sa) femtosecond pulsed laser (Chameleon Vision II, Coherent, Santa Clara, CA, USA) was utilized at a wavelength of 800 nm for MT severing. The beam was coupled to the bleaching port of the microscope. The pulsed laser light was reflected on the objective with a long pass dichroic mirror LP690.

Ablation was performed on user-defined, ellipse-shaped region of interest, ~0.3 μm wide and 1 μm long with the major axis perpendicular to the K-fiber. The system was controlled with the ZEN 2010 software (Zeiss).

Successful severing of the K-fiber in all experiments was identified by rapid depolymerization of the K-fiber fragment attached to the spindle pole, as well as from changes in the orientation of the short K-fiber stub that remained attached to the kinetochore (Elting et al., 2014; Sikirzhytski et al., 2014).

Imaging Combined with Photoactivation

Photoactivation experiments without laser ablation were performed on Leica TCS SP8 X laser scanning confocal microscope with a HC PL APO 63x/1.4 oil immersion objective (Leica, Wetzlar, Germany) heated with an objective integrated heater system (Okolab, Burlingame, CA, USA). During imaging, cells were maintained at 37°C in Okolab stage top heating chamber (Okolab, Burlingame, CA, USA). For excitation, a 488-nm line of a visible gas Argon laser and 594-nm line of white light laser (WLL) were used for GFP and mCherry, respectively. GFP and mCherry emissions were detected with HyD (hybrid) detectors in ranges of 498–560 and 608–676 nm, respectively. Pinhole diameter was set to 0.8 μm and pixel size was 84 nm. Images were acquired at 5-7 focal planes with 0.5 μm spacing using 1000 Hz bidirectional scanning. Time interval between Z-stacks was 20-30 s. For photoactivation of fluorescence of PA-GFP, a 405-nm laser diode was used. Photoactivation was performed using bleachpoint option in software, with duration of pulse set to 100 ms. The system was controlled with the Leica Application Suite X software (LASX, 1.8.1.13759, Leica, Wetzlar, Germany).

Transfection

U2OS cells were transfected by electroporation using Nucleofector Kit R (Lonza, Basel, Switzerland) with the Nucleofector 2b Device (Lonza, Basel, Switzerland), using X-001 program. Transfection protocol provided by the manufacturer was followed. Cells were transfected with mCherry-PRC1 plasmid provided by Casper C. Hoogenraad (Utrecht University). 1×10^6 cells and 1.5 μg of plasmid DNA were used. Transfection of U2OS line cells was performed 25–35 h before imaging.

Immunostaining

Cells were fixed in ice-cold methanol (100%) for 2 min and washed with PBS. To permeabilize cell membranes, cells were incubated in triton (0.5% in PBS) for 25 min at room temperature. Unspecific binding of antibodies was blocked in blocking solution (1% normal goat serum (NGS) in PBS) for 1 h at 10°C. Cells were incubated in 250 μL of primary antibody solution (4 μg/ml in 1% NGS in PBS) for 48 h at 10°C. Rabbit polyclonal anti-α-tubulin C-terminal antibody (SAB4500087, Sigma-Aldrich) was used. After washing of primary antibody solution, cells were incubated in 250 ml of the secondary antibody solution (4 μg/ml in 2% NGS in PBS; Alexa Fluor-405 F-conjugated donkey anti-rabbit IgG, ab175649; Abcam, Cambridge, UK) for 1 h at room temperature, protected from light. After each incubation step, washing was performed three times for 5 min in PBS softly shaken at room temperature.

Protein Depletion and Inactivation Experiments

For all siRNA treatments, 2×10^5 and 1×10^5 cells were seeded and cultured in 2 ml DMEM medium with same supplements (as above) at 37°C and 5% CO2 on 35 mm glass coverslip uncoated dishes with 0.17mm (#1.5 coverglass) glass thickness. After one-day growth, at ~50–60% confluency cells were transfected with 100 nM (except Kif15: 60 nM) raw targeting or non-targeting siRNA constructs diluted in a Opti-MEM medium (Life Technologies, Waltham, MA, USA). Transfection was performed using Lipofectamine RNAiMAX Reagent (Life Techologies). The constructs used were as follows: human MKLP-1 siRNA (sc-35936), human KIF15 siRNA (sc-78517) and control siRNA-A (sc- 37007), from Santa Cruz Biotechnology (Santa Cruz, CA, USA). 3h prior to imaging, the medium was replaced with Leibovit's (L-15) CO2-independent medium (Life Technologies), supplemented as above. The cells were imaged 24 or 48 hours after transfection. To inhibit Eg5, STLC (Sigma-Aldrich) was added to cells in L15 (see previous paragraph) 5 min before imaging at 40 μM (10 mM DMSO stock). To probe bipolar spindles with inhibited Eg5, we added 40 μM STLC after spindle formation (in metaphase), which preserves bipolarity (Cameron et al., 2006). All protein depleted cells were imaged by acquiring 8-12 focal planes with 0.5 μm z-spacing. Time interval between Z-stacks was 15 s. All other imaging parameters were the same as described for laser ablation experiments. We observed that inhibition of MKLP1 blocked normal progression of cytokinesis that resulted in formation of binucleated cells. We have observed an increase of 81% in the number of binucleated/multinucleated cells in MKLP1 siRNA-treated samples (calculated from 88 cells) after 48h in comparison with the samples treated with control siRNA (calculated from 92 cells), similar to previous observations (Fontijn et al., 2001). In experiment where KIF15 was inhibited by siRNA treatment, we observed rapid collapse of metaphase spindle upon 40 μM STLC treatment, as reported previously (van Heesbeen et al., 2014).

Theory

In our one-dimensional model, we describe a system consisting of 2 pairs of sister kinetochores, K-fibers which connect kinetochores and spindle poles, and MTs of the bridging fiber which extend from the opposite poles and interdigitate in the middle (Figure 5A). The positions of one kinetochore pair and poles are denoted $x_k^{\pm}$, and $x_p^{\pm}$, respectively. The positions of K-fibers and bridging fibers, $x_{kf}^{\pm}$, and $x_{br}^{\pm}$, respectively, are taken as an arbitrary position along their lattice, rather than the position of their ends, because their ends are dynamic. Superscripts + and − denote the right and left sides, respectively. The length of the microtubule overlap within the bridging fibers is denoted l_0.

The movement of the kinetochore at time t is calculated from a balance of a viscous friction and the force generated by the kinetochore $F_k^{\pm}$,

$$\xi_k \frac{dx_k^{\pm}}{dt} = F_k^{\pm}. \quad \text{(Equation 1)}$$

Here, the chromosome drag coefficient is denoted ξ_k. The force generated by the kinetochore depends on the velocity of the kinetochore with respect to the K-fiber lattice, which we describe by a linear relationship, $F_k^{\pm} = f_k\left(\pm 1 - \frac{v_k^{\pm} - v_{kf}^{\pm}}{v_{k0}}\right)$. Here, f_k denotes the stall force and v_{k0} the velocity without a load. Velocities are calculated as time derivatives $v_i^{\pm} = dx_i^{\pm}/dt$, where i = k, kf, br, p.

The movement of the K-fiber is driven by forces exerted by molecular motors distributed along the K-fiber, $F_m^{\pm}$, at the pole, $F_{pk}^{\pm}$, and at the kinetochore, whereas its sliding with respect to the bridging fiber is damped by passive crosslinking proteins,

$$N_c^{\pm}\xi_c \frac{d\left(x_{kf}^{\pm} - x_{br}^{\pm}\right)}{dt} = F_m^{\pm} + F_{pk}^{\pm} - F_k^{\pm}. \quad \text{(Equation 2)}$$

The number of passive cross-linkers distributed along the parallel overlap of a K-fiber and a bridging fiber is calculated as $N_c^{\pm} = \pm n_c(x_p^{\pm} - x_k^{\pm})$ with a constant linear density n_c and the length of the K-fiber $\pm(x_p^{\pm} - x_k^{\pm})$. The parameter ξ_c denotes the friction coefficient of a crosslinking protein. The forces of the motors distributed along the antiparallel overlap of a bridging fiber and a K-fiber depend on the velocity of the K-fiber with respect to the bridging fiber $F_m^{\pm} = N_m^{\pm} f_m\left(\pm 1 - \frac{v_{kf}^{\pm} - v_{br}^{\mp}}{v_m}\right)$, and the forces at the poles depend on the velocity of the K-fiber with respect to the pole $F_{pk}^{\pm} = f_p\left(\pm 1 - \frac{v_{kf}^{\pm} - v_p^{\pm}}{v_{p0}}\right)$. We used linear force-velocity relationships, where f_m and f_p denote stall forces and v_m and v_{p0} velocities without a load. The number of motors is given by $N_m^{\pm} = n_m(l_0/2 \mp x_k^{\pm})\theta(l_0/2 \mp x_k^{\pm})$, where n_m is the linear density of motors and the Heaviside function θ ensures that the antiparallel overlap exists.

The movement of the bridging MTs is driven by the force exerted by motors distributed along the antiparallel overlap of bridging MTs, F_{br}, along the antiparallel overlap of the bridging fiber and the K-fiber, and at the pole, $F_{pb}^{\pm}$. These forces are balanced by the friction that occurs when the bridging fibers slide with respect to K-fibers,

$$N_c^{\pm}\xi_c \frac{d\left(x_{br}^{\pm} - x_{kf}^{\pm}\right)}{dt} = \pm F_{br} - F_m^{\mp} + F_{pb}^{\pm}. \quad \text{(Equation 3)}$$

The force exerted in the overlap of bridging MTs depends on their relative velocities $F_{br} = N_{br} f_m\left(1 - \frac{v_{br}^{+} - v_{br}^{-}}{v_m}\right)$. The force at the pole depends on the velocity of the bridging fibers with respect to the poles $F_{pb}^{\pm} = f_p\left(\pm 1 - \frac{v_{br}^{\pm} - v_p^{\pm}}{v_{p0}}\right)$. The number of the motors in the overlap of bridging MTs is given by $N_{br} = n_m l_0$.

The movement of the poles is driven by the forces exerted by K-fibers and bridging fibers, which are balanced by viscous friction, with a drag coefficient of the pole denoted ξ_p,

$$\xi_p \frac{dx_p^{\pm}}{dt} = -\left(F_{pk}^{\pm} + F_{pb}^{\pm} + F_{pk}^{'\pm} + F_{pb}^{'\pm}\right). \quad \text{(Equation 4)}$$

The forces exerted by the second pair of K-fibers, $F_{pk}^{'\pm}$, and bridging MTs, $F_{pb}^{'\pm}$, are calculated by using Equations (1), (2), and (3) which are modified by adding a prime symbol to all variables.

Choice of Parameter Values

We varied the model parameters given in Figure 5B, starting from the most biologically relevant ones, see Figure S5A. We tested their influence on different velocities. By changing the density of sliding motors n_m, we found that above $n_m = 10\ \mu m^{-1}$ the velocity of the bridging microtubule is almost constant, so we chose a larger value (Figure S5A (i)). By changing the velocities v_{k0}, v_m, v_{p0}, we found that the only parameter that significantly influences the velocity of the bridging microtubule is the motor velocity without a load, v_m (Figure S5A (ii)). Hence, we set the value of the parameter v_m to reproduce the measured velocity of the bridging microtubule. Depolymerization velocity at the pole without a load, v_{p0}, is set to reproduce the measured velocity of the pole (Figure S5A (iii)). Depolymerization velocity at the kinetochore without a load, v_{k0}, is set to reproduce the measured velocity of the kinetochore (Figure S5A (iv)). The parameters describing stall forces, f_m, f_p and f_k, do not affect the kinetochore velocity significantly (Figure S5A (v)). The values of f_m and f_k were taken from the literature, whereas for f_p we chose a similar value. The parameters describing chromosome and spindle pole drag, ξ_k and ξ_p, have a minor influence on kinetochore velocity (Figure S5A (vi)). The value of ξ_k was taken from the literature, whereas for ξ_p we chose a 100 times larger value because of the size of the spindle pole. The value of the parameter describing passive cross-linker friction, $\xi_c n_c$, is chosen to overcome the drag force of the chromosome, i.e., $\pm(x_p^{\pm} - x_k^{\pm}) \cdot \xi_c n_c \gg \xi_k$.

QUANTIFICATION AND STATISTICAL ANALYSIS

The time of anaphase onset for each individual cell was defined as the time point immediately prior to the separation of sister chromatid populations as annotated manually using visual inspection based on the distance between the sister kinetochore groups. Time intervals in which the velocities were calculated for different experiments (one, two and three minutes) were chosen based on the criteria that they contain the majority of data. During the measurements of kinetochore velocity with respect to the midpoint we observed that the kinetochore whose K-fiber was severed showed a short delay (30.00±6.43 s, n=39) in the onset of movement with respect to its sister kinetochore. In this case, the beginning of anaphase was defined for each kinetochore individually as they started to move.

Image processing was performed in ImageJ (National Institutes of Health, Bethesda, MD, USA). Quantification and statistical analysis were performed in MatLab (MathWorks, Natick, USA).

Kinetochores were tracked in time using Low Light Tracking Tool (LLTT), an ImageJ plugin (Krull et al., 2014). Tracking of kinetochores in the x, y plane was performed on individual imaging planes or on maximum-intensity projections of up to three planes. The position in z direction was ignored because it had a small contribution to the kinetochore movement. In order to obtain optimal tracking results, it was necessary to define good intensity offset in the channel with fluorescently labeled kinetochores. The intensity offset was defined by measuring the mean intensity around kinetochores in the first frame before ablation using 'freehand selection' tool in Fiji. Sometimes, when photobleaching was prominent, bleach correction using Histogram Matching Method in Fiji was done to compensate for a decrease in background intensity in time. Also, it was necessary to define EMCCD gain and Electrons per A/D count of the used EMCCD camera to correct the measured flux of the object and background noise. The EMCCD-GaussianML tracking algorithm method was used (Krull et al., 2014) because it yielded more precise results compared with Gaussian-ML method, especially in situations when fast movement of the tracked object occurred (on a scale of micron per frame or more). All tracked objects were double checked by eye to ensure that tracking was accurate, because it was inaccurate in situations of an uneven intensity of tracked objects and in situations when multiple similar objects appeared in close proximity. If those cases were predominant, tracking was performed manually. σ value (standard deviation of the Gaussian used to approximate the Point Spread Function (PSF) of the tracked objects) was set to 1 to encompass just the tracked kinetochore.

Velocities of sliding and poleward flux in intact spindle were measured in 20 U2OS cells expressing CENP-A-GFP, mCherry-α-tubulin and photoactivatable (PA)-GFP-tubulin and 5 cells expressing only mCherry-α-tubulin and photoactivatable (PA)-GFP-tubulin. The measurements were done on both inner and outer bundles. Images were first smoothed using Gaussian Blur function in ImageJ with sigma set to 2.0. Segmented line was drawn from one spindle pole, across sister K-fibers and corresponding bridging fiber that spans between them, up to the opposite spindle pole. The intensity profile was taken along this line and positions of the peaks were measured. The thickness of the line was 3-5 pixels. The measurements were performed on maximum-intensity projections of up to three planes. All sliding measurements in protein inactivation/depletion experiments and in their appropriate controls were done in the interval when global kinetochore separation was between 3 and 7 μm. This interval was chosen because velocities of kinetochore and pole separation are linear during that period. Velocities where calculated as a linearly fitted change in the distance of photoactivated spots during 60 s from the initial photoactivation. Measurement of stability of photoactivation of the midzone bundles was calculated as the ratio of the area under the photoactivated midzone bundles in the 60 s after photoactivation and at the moment of photoactivation (0 seconds). The signal intensity of a cross-section of midzone bundles was measured in ImageJ by drawing a 5-pixel-thick line. The intensity profile was taken along the whole midzone region and the mean value of the background signal present in the cytoplasm was subtracted from it.

The attached kinetochore-photoactivated stub tip distance was measured in 9 U2OS cells expressing CENP-A-GFP, mCherry-α-tubulin and photoactivatable (PA)-GFP-tubulin. Images were first smoothed using Gaussian Blur function in ImageJ with sigma set to 1.5. Segmented line was drawn from one kinetochore, across the bridging fiber and the corresponding sister kinetochore to the photoactivated tip of the stub. The intensity profile was taken along this line and positions of the peaks were measured. The thickness of the line was 3-8 pixels. The measurements were performed on maximum-intensity projections of up to three planes.

The contour of displaced element after ablation was tracked in every time frame by using the Multi-point tool in Fiji (Figure 3A). Such measurement was done on individual imaging planes or on the maximum-intensity projections of up to five planes. A typical distance between the neighboring points on the contours was $\sim$1 μm. The measurement was done from the spindle pole far from the ablation site, along the intact K-fiber, to the tip of the K-fiber stub with one extra point on the spindle pole close to the ablation site (Figure 3A). From the obtained x and y coordinates, the distances between the points (intact spindle pole-stub tip, intact spindle pole-attached kinetochore, spindle pole close to ablation-detached kinetochore, attached kinetochore-stub tip, attached kinetochore-midpoint, detached kinetochore-midpoint) were quantitatively described.

To estimate the extent of depolymerization at the newly created minus end of the K-fiber stub, we used the side-effect of ablation laser that sometimes photoactivated PA-GFP-tubulin at the tip of the stub (Figure S3D). The photoactivated spot remained stable for 118.13±14.01 s (n=9) during anaphase even though the stub length simultaneously decreased (Figure S3D), indicating that the stub did not depolymerize at the minus end. Thus, stub shortening is a result of depolymerization at the plus end, i.e., Pac-Man activity.

Bridging fiber thickness measurement was performed on the side of the spindle where the ablation was performed, in the channel with fluorescently labeled MTs. Such measurement was done on individual imaging planes or on the maximum-intensity projections of up to three planes in the first frame after the ablation and the third frame from the start of the anaphase. In these planes, we could discern sister K-fibers without interference from neighboring fibers. The signal intensity of a cross-section of a bridging fiber (I_b) was

measured in Fiji by drawing a 3-pixel-thick line between outermost sister kinetochores and perpendicular to the line joining the centers of the two kinetochores. The intensity profile was taken along this line and the mean value of the background signal, present in the cytoplasm around sister K-fibers (measured in Fiji by drawing a 5-pixel-thick line), was subtracted from it. The signal intensity of the bridging fiber was calculated as the area under the peak closest to the kinetochores using SciDavis (Free Software Foundation, Inc., Boston, MA, USA). The width of this peak was typically 0.7 μm. The signal intensity of the K-fiber and the bridging fiber together (I_{bk}) was measured in a similar manner, 1 μm away from attached kinetochore and perpendicular to and crossing the corresponding K-fiber. The signal intensity I_b was interpreted as the signal of the bridging fiber, and I_{bk} as the sum of the K-fiber signal and the bridging fiber signal (I_b+I_k) because of their lateral connection in that region (Kajtez et al., 2016). Also, due to the limited optical resolution in light microscopy, it was not possible to distinguish separate bridging and K-fiber intensities within the I_{bk}. We observed that after the cut the bridging fiber remained linked to the displaced sister K-fibers during the initial outward-directed movement (Figure 1A), as described previously (Kajtez et al., 2016).

Kymographs of CENP-A-GFP and/or mCherry-α-tubulin were generated in maximum-intensity projections of all planes using Low Light Tracking Tool (LLTT), an ImageJ plugin (Krull et al., 2014). For kymographs where displaced kinetochores are presented in magenta, the displaced kinetochores traces where obtained by manually tracking the pair of sister kinetochores using LLTT. Obtained traces where overlaid with automatic traces of all kinetochore pairs in a cell generated by LLTT and shown in gray. Graphs were generated in Matlab. On the box plots the bottom and top edges of the box indicate the 25th and 75th percentiles, respectively. The whiskers extend to the most extreme data points not considered outliers, and the outliers are plotted individually using the '+' symbol. Outliers are defined as points greater than q3 + 1.5 × (q3 – q1) or lower than q1 – 1.5 × (q3 – q1) where q1 and q3 are the 25th and 75th percentiles of the sample data, respectively. Black solid lines indicate median values. p values were obtained using unpaired two-sample Student's t-test (significance level was 5%). When comparing the same parameters cell by cell, we used paired two-sample Student's t-test (significance level was 5%). Regarding data on Figure 5H, the y-axis coordinates were obtained by linear fitting every four points on average curve represented on Figure S5E. The x-axis coordinates were obtained by averaging every four points from average curve represented on Figure S5D.

Images of cells in figures were rotated so the spindle long axis is aligned horizontally, and ImageJ was used to scale the images and adjust brightness and contrast. Images where two or more channels are present are composites of individual channels. Kymographs and all quantitative analysis were done on raw images. Smoothing of images was done using Gaussian blur function in Fiji (σ=1.5-2.0). Figures were assembled in Adobe Illustrator CS5 and Adobe Photoshop CS5 (Adobe Systems, Mountain View, CA, USA). Data are given as mean±s.e.m., unless otherwise stated.